Vegetation and climate dynamics at the dawn of human settlement: multiproxy palaeoenvironmental evidence from the Hashilan Wetland, western Iran

Vegetation and climate dynamics at the dawn of human settlement: multi-proxy paleoenvironmental evidence from the Hashilan Wetland, western Iran

Reza Safaierad [1, *], Roger Matthews [2, *], Lydie Dupont [3,a], Bernd Zolitschka [4], Elena Marinova [5], Morteza Djamali [6], Christoph Vogt [7], Ghasem Azizi [8], Hamid A.K. Lahijani [9], Wendy Matthews [2]

[1]Clay, Geochemistry and Sedimentary Environments (AGEs), Department of Geology, University of Liège, B-4000, Liège, Belgium
[2]Department of Archaeology, University of Reading, Reading, UK
[3]MARUM–Center for Marine Environmental Sciences, University of Bremen, D-28359 Bremen, Germany
[4]University of Bremen, Institute of Geography, GEOPOLAR, Bremen, Germany ORCID: 0000-0001-8256-0420
[5]Laboratory for Archaeobotany Baden-Württemberg State Office for Cultural Heritage, Fischersteig 9, 78343, Gaienhofen, Hemmenhofen, Germany
[6]Institut Méditerranéen de Biodiversité et d'Ecologie-IMBE (Aix Marseille Univ, Avignon Université, CNRS, IRD), Europôle de l'Arbois, 13545 Aix-en-Provence, France
[7]Crystallography & Geomaterials Research, FB05 Geosciences & MARUM, University of Bremen, Bremen, Germany
[8]Department of Physical Geography, Faculty of Geography, University of Tehran, Tehran, Iran
[9]Iranian National Institute for Oceanography and Atmospheric Science, Tehran, Iran
[a]Present address: Hendrik Werkmanstraat 5, 1061VA Amsterdam
[*] Corresponding authors:
Reza Safaierad Safaierad.reza@gmail.com; and Roger Matthews; r.j.matthews@reading.ac.uk

Abstract

The scarcity of high-resolution paleoclimate records from the interior of West Asia has limited our understanding of the mechanisms of past climate change and their potential impacts on early human societies of the Eastern Fertile Crescent. Here, we present a multiproxy sedimentological, geochemical and palynological record from the Hashilan Wetland in the central Zagros Mountains, spanning the time interval from 22 to 2.2 kcal BP. Our results indicate a cold, dry climate for the Last deglaciation (22 to 10 kcal BP) with amplified aridity during the Last Glacial Maximum, Heinrich Stadial 1, the Younger Dryas, and the 8.2 and 3.2 ka events. The Early Holocene (11.6 to 7.8 kcal BP) is characterized by prolonged dry summers, frequent spring/summer dust storms and restricted oak woodlands that gradually expanded as summers shortened toward the second half of the Holocene (<6 kcal BP). We show an out-of-phase Holocene moisture variation between the interior of West Asia and the Indian Summer Monsoon domain and conclude that summer insolation-driven latitudinal shifts of the Hadley cell played a key role in seasonality changes in the interior of West Asia by modulating strength and pathway of the subtropical high-pressure cells. Finally, we explore possible impacts of these changes on regional prehistoric human communities.

Keywords: Atmospheric dust, Holocene seasonality changes, Neolithic, vegetation dynamics, Zagros Mountains.

Introduction

West Asia is influenced by multiple atmospheric circulation systems including Mid-Latitude Westerlies (MLWs), Indian Summer Monsoon (ISM), Subtropical High Pressure cells (STHPs) and the Siberian Anticyclone, making it one of the most sensitive regions of the world to climatic changes (Jones et al., 2019) (Fig. 1 A). Variations in intensity and interactions of these climate systems induce major shifts in climate regimes that have strong impacts on terrestrial ecosystems of the region (Fleitmann et al., 2003; Sharifi et al., 2015; Hamzeh et al., 2016; Talebi et al., 2016; Sharifi et al., 2018; Gurjazkaite et al., 2018; Vaezi et al., 2019; Safaierad et al., 2020; Alinezhad et al., 2021; Arsalani et al., 2022).

The Zagros Mountains, being NW-SE orientated along the western part of the Iranian Plateau, have a great potential for late Quaternary environmental and climatic reconstructions. This mountain range acts as a geographical barrier against humid air masses that are brought eastwards by the MLWs and receives substantial amounts of orographic precipitation, which creates a hospitable environment for human occupation contrasting the surrounding deserts and drylands. Zagros deciduous woodlands and shrubs have become the dominant vegetation across the mountain range since the Mid-Holocene when the current climate regime was established (van Zeist and Wright, 1963). Terrestrial vegetation dynamics of the early postglacial period and particularly the timing of the Zagros woodland expansion would have influenced the socio-economy of human communities living in the area at the dawn of the Neolithic (~11.8-7.2 kcal BP) by shaping the availability of natural resources for pastoral and early sedentary communities (Matthews and Nashli, 2013) (Fig.1 B).

Reconstructing hydroclimatic variations during the last glacial-interglacial transition is thus of importance for understanding the environmental context of Neolithization in the Zagros Mountains, i.e., the social processes humans made while transitioning from mobile hunter-gatherer to sedentary farmer-herder communities. Ongoing research confirms that the Zagros range of western Iran and eastern Iraq is a core zone for an extremely early transition to settled village life, including the domestication of locally available plant and animal species (Matthews et al., 2020). The few previous investigations in NW Iran and the southern Zagros already revealed significant hydrological change during this transition (Aubert et al., 2017; Aubert et al., 2019). For more than a century there has been debate concerning the possible role of climate change as a factor in shaping the Neolithic transition across West Asia (Matthews and Nashli, 2013), including impacts of the cool-dry Younger Dryas stadial (YD: ~12.8-11.6 kcal BP) and of sudden cooling episodes such as the so-called 9.2 and 8.2 ka events (Flohr et al., 2016). The Hashilan Wetland

paleoenvironmental record covers this relevant timespan and is located close to key Early Neolithic archaeological sites with the potential to make a major contribution to these debates. This record can extend our current knowledge of environmental changes in the Zagros Mountains known from a few paleoenvironmental studies carried out on sediment cores from Lake Zeribar and Lake Mirabad in western Iran (van Zeist and Wright, 1963; Wasylikowa, 1967; van Zeist and Bottema, 1977; Griffiths et al., 2001; Stevens et al., 2001; Stevens et al., 2006; Wasylikowa et al., 2006). The chronology and mechanisms behind these changes are still poorly constrained. For instance, the reason for a ~4,500-year delay in deciduous woodland expansion reflected in the Early Holocene pollen assemblages from the Zagros-Anti-Taurus Mountains (van Zeist and Wright, 1963; van Zeist and Bottema, 1977; Wick et al., 2003) is not well understood. However, the mechanism proposed by Stevens et al. (2001) seems compelling, which attributes the delay to enhanced climate seasonality characterized by a hot, dry summer and concentrated precipitation in winter. Consistent with this mechanism, Djamali et al. (2010) using modern atmospheric data indicated that the northward expansion of the ISM changes climate seasonality in the Zagros-Anti-Taurus Mountains by reducing spring rainfall. The same mechanism could thus have been responsible for the delay in the expansion of Zagros oak woodlands in the Early Holocene. Due to the lack of high-resolution and well-dated Holocene sediment records representing a sufficiently large area in the Zagros Mountains, no solid evidence has yet been provided to test this hypothesis.

In this contribution, we present a new multi-proxy record including pollen and sedimentological data for the period between 22 and 2.2 kcal BP from the Hashilan Wetland, which is a karstic-spring carbonate wetland (Djamali et al., 2018) located in the central Zagros. In this study we aim at:

(I) Reconstructing the vegetation dynamics in the central Zagros region to close a gap in paleoenvironmental data during the late Pleistocene-Holocene (see e.g., European Pollen Database www.eauropeanpollendatabase.net).

(II) Situating the Hashilan record in a regional context to explore the driving mechanisms responsible for Holocene climate variability and atmospheric reorganization in the interior of West Asia.

(III) Investigating the potential impacts of dynamic paleoenvironmental factors on regional early human societies.

Study area

The Hashilan Wetland: its geological and hydrological setting

Hashilan Wetland is a vast karstic spring-fed carbonate wetland with an anastomosing fluvial pattern (Djamali et al., 2018) extending over 4.5 km^2 surface area and located 36 km northwest of Kermanshah City, western Iran (Fig. 2 A and B). This 'anastomosing carbonate wetland system' was formed at the emergence point of two karstic springs like many similar wetlands in the Zagros Mountains (Djamali et al., 2018). The very gentle slope of the plain, the high rate of biochemical carbonate precipitation in a densely vegetated environment, and the highly fluctuating water table contribute to the formation of palustrine carbonates, which show both sedimentary and pedogenic features (Alonso-Zarza, 2003; Djamali et al., 2018). During episodes of higher karstic spring discharge, water level rises and the small bog ridges (strings) become inundated whereas the larger island-like spots remain subaerial and above the water table.

Hashilan Wetland developed at the northern edge of the synclinal Allahyar-Khani Plain surrounded by Khorrin Mountains in the north and Veis Mountains in the southwest. Two karst springs are fed by the Khorrin karst aquifer, which originates in the massive limestone of Bisotun. With a thickness of ca. 2000 m, the pure Bisotun limestone is characteristic for well-developed karstic landforms (Bagheri-Seyedshokri et al., 2013). The Khorrin karst aquifer is recharged through water penetration into karrens, vertical and horizontal joints and cracks, and also directly from shafts and sinkholes. The hydrodynamic investigation of the Khorrin karst aquifer shows that the dynamic storage volume of the aquifer is very low, which results in fast discharge of water through karst springs (Bagheri-Seyedshokri et al., 2013). This prominent feature of the aquifer results in great water level variability and makes the wetland extremely sensitive to droughts. For instance, in response to a severe drought in 2007, the wetland area was reduced by about 47% compared to the previous year (Jafarbigloo et al., 2015).

Climate and vegetation

The mean annual precipitation (30-year average; 1988-2017) is 410 mm recorded in the nearest meteorological station at Kermanshah, located 36 km southeast of the wetland. March with a mean precipitation of 71.7 mm and July with less than 1 mm are the wettest and driest months, respectively. The mean annual temperature is 15.5 °C. January with a mean temperature of 2 °C and July with 29.3 °C are the coldest and warmest months, respectively. The dry season lasts about 5.5 months from mid-April until October, during which STHPs dominate the regional atmospheric circulation (Zarrin et al., 2010). Maximum dust storm activity occurs during late spring

and early summer (June and July) with the minimum in November (Zolfaghari and Abedzadeh, 2005). The main moisture sources for central Zagros precipitation are low-depression systems from the North Atlantic, the Mediterranean Sea and the Black Sea traveling eastwards with the mid-latitude westerlies (Alijani and Harman, 1985; Stevens et al., 2001). During boreal winter, STHPs weaken and shift southwards due to the latitudinal migration of the Intertropical Convergence Zone (ITCZ) and weakening of the Hadley cell, allowing the westerly depressions to penetrate into central Zagros causing precipitation through winter and spring. In addition, heavy rainfall may occur when the Sudan thermal low interacts with the eastern Mediterranean trough (Khoshakhlagh et al., 2008) transporting moisture from the Arabian Sea, the Red Sea and the Persian Gulf into the region (Khoshakhlagh et al., 2014).

In the Köppen climate classification system (Köppen, 1931), the study area has a Mediterranean-type climate and in the Global Bioclimatic Classification System it has a Mediterranean pluviseasonal-continental bioclimate (Djamali et al., 2011). This bioclimatic zone forms the dominant bioclimatic unit in the Zagros upland areas (Djamali et al., 2011). The Mediterranean continental bioclimate mostly corresponds to the Irano-Turanian floristic region (Djamali et al., 2012b), which covers the majority of SW Asia including the Hashilan Wetland (Zohary, 1973; White and Léonard, 1991)

To achieve a detailed understanding of the vegetation in the study area, we conducted a botanical survey in the wetland and in the surrounding mountains during the flowering season in spring. Based on our botanical survey the main vegetation types were described, of which a summary is presented here. The regional natural vegetation in the surroundings of the wetland has an open character and can be characterized as forest-steppe and warm-temperate shrublands. Common trees of the area are *Pistacia khinjuk*, *P. atlantica* subsp. *mutica* and *Crataegus azarulus* var. *aronia* growing between 1300 and 2000 m a.s.l. along with some species of *Prunus* shrubs, such as *P. scoparia* (wild almond) and *P. carduchorum*. At these altitudes, other shrubs such as *Cerasus microcarpa* and *Rhamnus kurdica* and herbaceous species, including species of *Echinops*, *Phlomis*, *Stachys*, *Onosma*, *Taraxacum*, *Salvia* and others, are the main constituents of vegetation. Oak woodlands (i.e., *Quercus brantii* Lindl.)—apart from sporadic tree stands on the northern slopes of the Khorrin Mountains—are absent in the Allahyar-Khani Plain and its surrounding mountains and the nearest open oak woodland is located about 30 km west of Hashilan Wetland.

In the zone between 2000 and 2500 m a.s.l., arboreal taxa such as *Acer monspessulanum* and *Lonicera nummulariifolia* sporadically occur. Above 2500 m a.s.l., the vegetation is treeless and displays a typical Irano-Turanian montane steppe with *Ferulago angulata*, *Prangos uloptera*,

Rheum ribes, *Euphorbia*, *Smyrniopsis aucheri* and *Astragalus caprine* being the dominant plant species.

Within the Hashilan Wetland, the peat strings are covered with marsh vegetation mostly consisting of members of the Cyperaceae family, namely, *Carex riparius*, *Cyperus longus, Juncus articulatus*. The submerged depressions (flarks) are dominated by *Phragmites australis, Typha latifolia, T. angustifolia and Sparganium erectum*. The less water-logged areas of the wetland are colonized by herbs such as *Mentha longifolia, Sium, Bidens tripartita, Epilobium hirsutum,* and *Ranunculus* spp. Scattered *Salix alba* trees are the only arboreal taxa growing on the wetland. The Allahyar-Khani Plain is intensively under cereal cultivation because of its highly fertile soil and availability of water.

Materials and Methods

All data that support this study have been published (Safaierad et al., 2023) and are available online.

Fieldwork and sampling

A 400-cm long sediment core (HW) was retrieved from the Hashilan Wetland (34° 34′ 55″ N, 46° 53′ 13″ E, 1310 m a.s.l.) using a Russian peat corer. The half-barrel cores were wrapped in plastic, placed in PVC core liners and stored at 4 °C. To enable precise identification of pollen grains, we collected about 90 flowering plant taxa during a botanical survey in the wetland and surrounding mountain areas. In this paper, we report about a 310-cm long section of the core covering the depth interval between 85 and 395 cm. Loss-on-ignition (LOI) and magnetic susceptibility (MS) of the same core section have previously been published in Safaierad et al. (2018). This study employs new sedimentological, geochemical and pollen analyses and improves the chronology with additional radiocarbon dates.

Radiocarbon dating

Seventeen samples including bulk organic sediments, seeds and charcoal fragments were submitted to the Beta Analytic Radiocarbon Dating Laboratory, Miami, USA (Table 1). The AMS ^{14}C dates were calibrated using the Northern Hemisphere terrestrial calibration curve IntCal20 (Reimer et al., 2020). The Bayesian age-depth model was generated using the rbacon package (Blaauw and Christen, 2011) and the RStudio software (R Development Core Team, 2013). The 95% confidence intervals are based on a 2σ range of average iterations. All ages are reported as thousand years before AD 1950 in kcal BP.

Magnetic susceptibility

MS of the core was measured using a Bartington MS2C sensor at the Marine Geology Division of the Iranian National Institute for Oceanography and Atmospheric Science (INIOAS). The down-core scanning was carried out in 1-cm increments.

Loss on ignition

Eighty-five samples of 1 g each were taken at 4-cm intervals from the 310-cm core sequence and analyzed to determine organic matter (OM), carbonate content ($CaCO_3$), and non-carbonate mineral matter (NCMM) of the sediments. The LOI was processed following the method proposed by Heiri et al. (2001). Samples were dried overnight at 105 °C and weighed. The dry samples were combusted at 550 °C for 4 hrs and at 950 °C for 2 hrs and percentages of OM and lost CO_2 were determined, respectively. The results of the LOI 950 °C were multiplied by 1.36 to express the carbonate content (Heiri et al., 2001). Finally, the percentage of NCMM (LOI residue) was calculated using the following formula:

NCMM = 100 – LOI550 – LOI950 * 1.36 (in %).

Pollen analysis

For pollen analysis, 34 subsamples (excluding barren pollen samples) of 1 cm^3 wet sediment were collected at 8 to 10 cm intervals. Standard analytical techniques (Faegri and Iversen, 1989) were applied for pollen extraction at the faculty of geography, University of Tehran and the Faculty of Geosciences, University of Bremen. Samples were treated with 10% KOH, 10% HCl, 37% HF and acetolysis. The pollen grains were extracted from the size fraction between 160 and 10 µm sieves and were mounted in silicone oil (2000 cs). Plant taxa collected during field work were identified and their flowers acetolyzed (Erdtman, 1960) to make a small reference collection. Pollen identifications were made using the pollen atlas of western Iran (van Zeist and Bottema, 1977) and our own pollen reference collection. At least 300 terrestrial (upland) pollen grains were counted per sample except for depths at 111 and 223 cm with poor pollen preservation. Aquatic pollen grains were excluded from the total pollen sum. The pollen diagram and the CONISS dendrogram were calculated and plotted by means of the TILIA software (Grimm, 1987; Grimm, 2011).

Elemental analysis by X-Ray Fluorescence (XRF) core scanning

To obtain qualitative information about their elemental composition, 76 samples were dried, ground and measured individually with an ITRAX XRF core-scanner (Cox Analytics) (Croudace

et al., 2006; Croudace et al., 2019) following the approach of Profe and Ohlendorf (2019) for measuring discrete samples. Analyses were carried out with the Molybdenum (Mo) X-ray tube with a voltage of 30 kV, a current of 40 mA and 100 s exposure time. XRF-scanning data are influenced by matrix effects related to grain size, porosity, water content, organic matter content, instrumental characteristics and others. As samples were ground and dry, the factors grain size, porosity and water content are negligible in this case. In general, the chemical composition obtained by the XRF core scanner is non-linearly correlated to elemental concentrations (Tjallingii et al., 2007; Croudace et al., 2019). Moreover, element intensities underlie the closed-sum effect, which inhibits multivariate statistical analyses (Martin‐Puertas et al., 2017). A solution for these limiting factors is available with the centered log ratio (clr), which normalizes data and determines relative changes in element composition resembling their chemical composition (Weltje et al., 2015). Moreover, clr transformation is consistent with the statistical theory of compositional data analyses (Aitchison, 1982; Weltje et al., 2015). Additionally, selected elements are displayed as element/element ratios.

Mineralogical analysis by X-Ray Diffraction (XRD)

Sixteen samples about 1 g of weight were dried at 50 °C for 48 hours. The dried samples were ground and homogenized using mortar and pestle. XRD analyses were carried out at the Crystallography and Geomaterials Group, Dept. of Geosciences, University of Bremen. The X-ray diffractograms have been measured on a Philips X'Pert Pro multipurpose diffractometer equipped with a Cu-tube (k_α 1.541, 45 kV, 40 mA), a fixed divergence slit of ¼°, a 16 samples changer, a secondary Ni-Filter, and the X'Celerator detector system. Measurements were performed as a continuous scan from 3–65° 2θ, with a calculated step size of 0.016° 2θ (calculated time per step was 100 s). Minerals were identified with the Philips/Panalytical software X'Pert HighScore™, which can also give a semi-quantitative value for each identified mineral on the basis of Relative Intensity Ratio (R.I.R)-values. The R.I.R.-values are calculated as the ratio between the intensity of the most intense reflex of a specific mineral phase and the intensity of the most intense reflex of pure corundum (I/Ic) referring to as the "matrix-flushing method" after Chung (1974).

Grain size analysis

Prior to grainsize analyses, OM was removed by H_2O_2 (30 %) and carbonates were destroyed with HCl (10 %) from each of the 59 samples. For dispersion, 20 ml of Calgon [$(NaPO_3)n$] was

added and agitated overnight. On the next day, analyses were performed with a laser diffraction particle-size analyzer (Beckman Coulter LS 200) after ultrasonic treatment for 30 s. Each sample was measured at least four times for 60 s until a stable distribution was reached. Thereafter, the arithmetic mean was calculated for the best three sample runs. Grainsize distributions and all statistical grainsize parameters were calculated from the output of the LS 200 as geometric graphical measures according to Folk and Ward (1957) with the MS Excel-based macro Gradistat, Version 8.0 (Blott and Pye, 2001).

Results and interpretations

Chronology

The Bayesian age-depth model based on 11 calibrated ^{14}C dates (Table 1) is illustrated in Fig. 3. According to the age model, the Hashilan Wetland sediment core covers the period 22 to 2.2 kcal BP (at 85 cm). Of the seventeen ^{14}C age determinations (Table 1) six samples are obtained from roots and rhizomes of *Phragmites australis*, which are younger by several thousand years than those of organic sediment from the same depths. Therefore, we determined them as outliers (Fig. 3). Penetration of roots and rhizomes of such deeply-rooted plants into underlying sediments is a common cause of age inversion in wetland sediments (Howard et al., 2009) and has recently been reported from similar deposits in the southern Zagros Mountains (Djamali et al., 2018). The reason for exclusion of these dates from the age-depth model is that they do not follow the trend, characterized by substantial changes in sedimentation rates, but also indicate an age reversal at 197 cm depth. However, the lithological structure of the sediment core from 283 cm upwards, which is composed of compacted gyttja (Fig. 3), reflects a calm depositional condition with no signs of sudden changes. In contrast, dates of organic sediment indicate a reliable decreasing trend from the bottom of the core upward, which is consistent with the lithological structure of the sediment core. Although the presence of dissolved old carbon in lake water of carbonaceous basins can affect radiocarbon dates of bulk sediments and results in too old ages, dating of organic sediment fractions can minimize the effect of old carbon. In the Hashilan sediment core, the main source of organic content, as indicated by the pollen record (Fig. 5), are plants of the Cyperaceae family. Their photosynthetic mechanism depends on atmospheric CO_2 rather than on dissolved old carbon. The consistent dates of the organic sediment at 395 cm and the Cyperaceae seeds at 394 cm also suggest the reliability of bulk sediment dates. Furthermore, the

reliability of our chronology is supported by the temporal link between our record and regional records (see Fig. 6 and Fig.7).

Sedimentology

The Hashilan Wetland sediment core is characterized by two markedly different lithological units. The basal part of the core from 395-283 cm (22-15.5 kcal BP) is composed of highly calcareous sediments, which are overlain by organic gyttja (organic-rich lake mud) from 283 to the top of the record at 85 cm (15.5-2.2 kcal BP) (Fig. 4). The gyttja, however, embraces a carbonate-rich layer between 260 and 250 (13-11.9 kcal BP), and two mineral-rich layers from 225 to 206 cm (10.4-9.5 kcal BP) and 195 to 170 cm (9-7.8 kcal BP). To investigate these lithological changes, we employ multiple sedimentological indices including grain size, LOI, XRF geochemistry, MS, and XRD mineralogy (Fig. 4).

XRF geochemistry yielded ten elements (Ca, Ti, Cr, Mn, Fe, Ni, Zn, Rb, Sr and Zr) with reliable and significant abundances (>2500 counts per second). These are categorized into two different groups of carbonaceous and siliciclastic elements with Ca and Sr (r = 0.99; Tab. 2) being positively correlated representing the carbonaceous group, while the rest falls into the siliciclastic group with many of these elements being highly correlated (Tab. 2). Ca and Ti, which are highly and negatively correlated (r = -0.93), are selected as representatives for the carbonaceous and siliciclastic groups, respectively. The carbonaceous sediments are derived from adjacent limestones and transported via karstic springs and runoff, whereas siliciclastic sediments are mainly of remote (aeolian) origin. This is supported by mineralogical results indicating a significant presence of quartz and albite as well as clay minerals such as clinochlore, smectite, palygorskite and montmorillonite in the gyttja deposits, which all have been identified in dust loads originating from Iraq and the Arabian Peninsula (Najafi et al., 2014; Kumar et al., 2020). The silt-sized grains of the gyttja sections also support aeolian sources of the siliciclastic material. Instead, the notable presence of calcite in carbonaceous sediments (Fig. 4) confirms a local origin of the sediments. Coarsening of the sediments to sand-size in the calcareous sections is thus attributed to enhanced erosion in the catchment. Therefore, we interpret the Ti/Ca ratio as representing changes of aeolian versus runoff-related deposits in the sediment.

The Ti/Ca ratio covaries well with NCMM and MS profiles, which indicates that the influx of siliciclastic dust minerals into the wetland is responsible for increased MS. Hence, we use the better resolved MS record as a proxy for dust input into the Hashilan Wetland. Nevertheless, to

eliminate the possible diluting effect of calcareous sediments, we limit the applicability of the MS proxy to the Holocene gyttja section of the core (<11.9 kcal BP). Overall, based on variations of sedimentological indices, and in particular on the MS record for the Holocene, the Hashilan Wetland sediment core can be divided into five sedimentological zones.

Zone 1 (395-283 cm, 22 to 15.5 kcal BP)

This zone is characterized by highly calcareous (49% carbonate content), organic poor (4.6% OM) sediments (Fig. 4), comprising between 60 and 98% calcite (Fig. 4). Although a proportion of the calcite content is derived from biogenic sources such as ostracods, the sandy silts point to a local source transported via karstic springs and runoff into the wetland or possibly a shallow lake. The presence of a shallow lake during the dry glacial period is explained by the suppression of evaporation under cold climate conditions, a feature also seen at Lake Urmia, NW Iran (Djamali et al., 2008). The monotonous trends of all sedimentological indices show generally stable depositional conditions for this zone. The only notable change is the influx of coarse-grained sediments due to increased erosion between 22-20 kcal BP and 17-15.5 kcal BP corresponding with the Last Glacial Maximum (LGM) and Heinrich Stadial 1 (HS1; ~18-14.6 kcal BP), respectively.

Zone 2 (283-260 cm, 15.5 to 13 kcal BP)

In this zone, the lithology changes sharply to gyttja consisting of 25% OM and 11% carbonate content (Fig. 4), on average. A change in origin of the sediments from local to remote sources is reflected by the replacement of calcite by quartz (66%) and clinochlore (23%) (Fig. 4) that are responsible for elevated MS. As this zone broadly corresponds with the Bølling–Allerød interstadial (~14.7-12.9 kcal BP), an increase in temperature may have enhanced evapotranspiration that turned the pre-existing shallow lake into a humid wetland or palustrine environment. This interpretation is consistent with variations in diatom assemblages at Lake Zeribar showing an increase in temperature at 15.4 kcal BP (Wasylikowa et al., 2006).

Zone 3 (260-250 cm, 13 to 11.9 kcal BP)

This zone corresponds to the Younger Dryas (YD; ~12.8-11.7 kcal BP). It shows a recurrence of calcite deposition (25% of all minerals) (Fig. 4) in the wetland, leading to a drop in OM and MS (Fig. 4). The presence of smectite in this zone (8%) is associated with aeolian processes. Thus, the reduced MS does not reflect a decrease in dust input but a dilution effect of the non-magnetic calcite deposited at the same time. This interpretation is in agreement with an increase in dust deposition during the YD for West Asian records (Sharifi et al., 2015; Sharifi et al., 2018; Vaezi et

al., 2019; Safaierad et al., 2020). The increase in median grain size at the beginning of this zone points to increased erosion in the catchment at the beginning of the YD.

Zone 4 (250-140 cm, 11.9 to 6 kcal BP)

In this zone, the lithology alternates between gyttja and silty gyttja (Fig. 4) with notable contributions of aeolian clay minerals such as clinochlore, smectite, palygorskite and montmorillonite (Fig. 4). Increased intensity of MS from 10.6 to 9.5 and 8.8 to 8.1 kcal BP (Fig. 4) indicates elevated dust deposition in the Hashilan Wetland during the Early Holocene. An increase in grain size between 8.3 and 8 kcal BP (Fig. 4) can be attributed to both enhanced erosion and also stronger dust storms that transported coarse-grained silt and fine sand into the wetland. This interval is coeval with the 8.2-ka event, during which other West Asian records show enhanced dust input (Sharifi et al., 2015; Sharifi et al., 2018; Vaezi et al., 2019; Safaierad et al., 2020). In contrast, the decreased dust input between 9.5 and 8.8 kcal BP, centered at 9.2 kcal BP, is synchronous with a less severe cooling event in the Northern Hemisphere known as the 9.2-ka event (Flohr et al., 2016). The dust input decreases after 7.8 kcal BP and shows a less pronounced peak between 6.9 and 6.6 kcal BP (Fig. 4).

Zone 5 (140-85 cm, 6 to 2.2 kcal BP)

A decrease in NCMM, the Ti/Ca ratio and MS values accompanied by an increase in OM signifies markedly reduced dust input and more stable environmental conditions in the Hashilan Wetland after 6 kcal BP (Fig. 4). A notable drop in MS between 3.3 and 2.9 kcal BP is associated with increased erosion and influx of coarse-grained sediments with calcite from the catchment into the wetland, which is synchronous with arid conditions identified in a peat core from SE Iran (Vaezi et al., 2022) and increased aeolian deposition in Lake Neor, NW Iran (Sharifi et al., 2015). Interestingly, similar to the other episodes of enhanced erosion identified in the Hashilan Wetland sediment core, this episode is also coeval with a cold and dry climate event known as the 3.2-ka event (~3.3 to 2.9 kcal BP) that influenced Late Bronze and Early Iron Age communities in different regions including southwestern Asia (Neumann and Parpola, 1987; Alpert and Neumann, 1989; Shaikh Baikloo Islam, 2021; Vaezi et al., 2022), the eastern Mediterranean (Kaniewski et al., 2019), and western Europe (Molloy, 2022).

Palynology

Ninety-two pollen types of 15 trees, 72 herbs and shrubs, and 5 aquatic plant taxa were identified in the samples from the Hashilan Wetland sediment core. A simplified pollen percentage diagram

(Fig. 5) represents two major local pollen assemblage zones (LPAZs). Both are divided into sub-zones by means of the CONISS clustering method (Grimm, 1987) (Fig. 5).

LPAZ A

The LPAZ A (22 to 9.8 kcal BP) is characterized by high percentages of Amaranthaceae (now embracing formerly Amaranthaceae and Chenopodiaceae) pollen of up to 65% as well as Poaceae (16.8%) and *Artemisia* (16.2%), with a significant amount of Asteraceae (e.g., *Cousinia;* 1.5%) and Plantaginaceae (e.g., *Plantago coronopus*-type; 1.5%) along with less *Ephedra*. Cyperaceae is the only dominant wetland pollen taxon and its abundance shows significant changes in LPAZ A. In addition to Cyperaceae, pollen of *Typha/Sparganium*-type occurs in low abundance (less than 2%), though it has a relatively constant presence. The insignificant abundance of tree pollen not exceeding 2% on average reflects a nearly treeless landscape during this time. Altogether, such a pollen assemblage indicates the dominance of Irano-Turanian mountain dry steppe in the uplands of the region and a sparse aquatic vegetation within the wetland (supported by the low OM content) during the period 22-9.8 kcal BP. The Hashilan Wetland record registers a continuous presence of *Cousinia* species during the late glacial, corroborating other glacial pollen records of the interior of West Asia (Djamali et al., 2012a), which accentuates the significant role of this plant in the central Zagros Mountains during the late Pleniglacial and the deglaciation.

The fluctuations in abundance of Amaranthaceae and Poaceae pollen possibly reflect a local origin in contrast to those of *Artemisia*. Changes in the abundance of Amaranthaceae and Poaceae plants can be associated not only with changes in climate conditions but also with water table variations. The halophilous and halotolerant species of Amaranthaceae can dominate on saline soils of the surrounding plain as well as on the margin of the wetland during shorter periods of waterlogging (Dehghani et al., 2017). On the other hand, wetland Poaceae (e.g., *Phragmites australis)* can develop in shallow littoral waters emerging by longer waterlogging during episodes of an elevated water table (Djamali et al., 2016). As a result, variations in abundance of these plants are, to some extent, controlled by changes in wetland hydrology. Instead, *Artemisia* as an upland vegetation element, is independent of changes in waterlogging, better represents the regional upland vegetation and slight variations in its pollen reflect minor changes in regional vegetation throughout LPAZ A.

An increase in the surface soil-salinity is indicated by the low abundance of pollen of the *Typha/Sparganium*-type, which are sensitive to soil salinity (Glenn et al., 1995). The increased

salinity can be associated with a decrease in surface leaching due to droughts, supporting the idea of the expansion of halophytic Amaranthaceae species around the wetland in LPAZ A. Based upon changes in relative abundance of the most common pollen taxa, LPAZ A is divided into four sub-zones.

LPAZ A1 (22 to 21 kcal BP)

The main terrestrial pollen grains of this sub-zone are Amaranthaceae (45%), Poaceae (20%), and *Artemisia* (16%). One noticeable feature of this sub-zone is the high abundance of Cyperaceae pollen, which reach up to 50% in the lowermost pollen sample of the record. However, highly calcareous sediments with low OM content (6%) of this sub-zone points to the lack of a dense carpet of Cyperaceae at the coring site that may be placed inside a shallow lake surrounded by a palustrine environment.

LPAZ A2 (21 to 18 kcal BP)

The major terrestrial pollen percentages are similar to sub-zone A1, reflecting a dry *Artemisia*-Amaranthaceae steppe. However, a notable decrease in abundance of Cyperaceae pollen which reach its minimum (ca. 7%) throughout LPAZ A, is the distinguishing feature of this sub-zone from the underlying sub-zone. Similar sediment composition and terrestrial pollen abundances of LPAZ A1 and A 2 implies that the higher abundance of Cyperaceae pollen in LPAZ A1 can be indicative of a larger palustrine environment around the shallow lake due to extended inundation.

LPAZ A3 (18 to 14.5 kcal BP)

This sub-zone is distinguished by a significant increase in Amaranthaceae pollen reaching a maximum abundance of 65% at the expense of Poaceae, indicating an increase in aridity and/or soil salinity. This pollen sub-zone coincides with HS1, during which a massive discharge of icebergs into the North Atlantic caused a pervasive cooling in the Northern Hemisphere (Heinrich, 1988; Bond et al., 1992).

LPAZ A4 (14.5 to 9.8 kcal BP)

This sub-zone covers the Late Glacial and the first two millennia of the Holocene. In the lower half, which corresponds to the Bølling–Allerød (B/A) interstadial, Poaceae pollen increase at the expense of Amaranthaceae. Cyperaceae increase distinctly, pointing to reduced aridity and soil salinity. After ~13 kcal BP, which broadly corresponds to the onset of the YD, the abundance of Poaceae, *Artemisia* and Cyperaceae and increasing Amaranthaceae suggest higher aridity and continentality. A notable increase in pollen of the *Polygonum aviculare* and *Senecio-Filago*-type

may indicate that the increased climate aridity was accompanied by fluctuations in water table leading to the spread of the latter plants at the seasonally exposed/inundated littoral zones of the wetland.

Multiple forms of evidence, such as the presence of calcareous sediments, abundant ostracods (observed by visual inspection of sediments under a microscope) and very good pollen preservation in the lower part of the sediment core (395-283 cm, from 22 to 15.5 kcal BP) suggest the presence of a shallow lake around the coring site prior to the B/A warm period. During cold periods—despite a substantial decrease in precipitation—the majority of precipitation most likely occurred as winter snowfall (Wright Jr, 1962). Gradual melting of the snow lasts into the warm season along with a substantial suppression of the evapotranspiration rate could have supported the existence of the shallow lake. The higher water level of the lake (compared to wetland) would have prevented the growth of Cyperaceae inside the lake or at the coring point, as reflected by low OM. During warm periods when precipitation increased, e.g., at the onset of the B/A, a decrease in snowfall and an increase in evapotranspiration would have turned the shallow lake into a wetland by lowering the water table that favors the expansion of Cyperaceae and the formation of gyttja.

With the onset of the Holocene, a significant change occurs in pollen preservation. Between 11.5 and 7.8 kcal BP, pollen grains decayed during the long exposure of the wetland surface to air, except for a short intervening interval between 10.3 and 9.8 in which a small number of pollen grains have been poorly preserved. The similarity of the pollen taxa preserved in this section and the previous sub-zones classifies this section within the major pollen assemblage of LPAZ A and indicates the persistence of the dry *Artemisia*-Amaranthaceae steppe in the region until at least the first two millennia of the Holocene. This is consistent with the results of the existing pollen records from the Zagros-Anti-Taurus Mountains showing dominance of steppe elements in the vegetation composition until about 10 kcal BP (van Zeist and Bottema, 1977; Wick et al., 2003). The increase in abundance of pollen of the drought-tolerant and semi-desert shrub *Ephedra* (*E. distachya*-type and *E. fragilis*-type) indicates an increase in aridity and/or protraction of the dry season during the Early Holocene leading to intermittent desiccation of the wetland. Nevertheless, a sudden increase in abundance of the *Typha/Sparganium*-type may indicate reduced soil salinity after 10.3 kcal BP.

LPAZ B

In general, the transition from LPAZ A to B is marked by a major change in vegetation composition.

LPAZ B1 (7.8 to 6 kcal BP)

In LPAZ B1, a prominent increase in the abundance of Poaceae pollen (up to 55%) at the expense of *Artemisia* (2%) and Amaranthaceae (12%), as well as the continuous and slowly increasing abundance of pollen of *Quercus* and *Pistacia* indicates a major change in the regional vegetation from a steppe to a steppe-forest dominated by grasses. The simultaneous increase in pollen of grasses and aquatic/wetland plants such as Cyperaceae, *Typha/Sparganium*-type, *Typha latifolia*-type and Ranunculaceae shows increased humidity and reduced soil salinity. It also suggests that a portion of the grass pollen comes from local *Phragmites australis*. However, attempt to disentangle the question of how much of the grass pollen are of local origin is hampered by the fact that pollen of *Phragmites australis* cannot reliably be distinguished from upland grasses. Overall, pollen-inferred vegetation changes in this zone indicate a climate amelioration and increasing humidity after 7.8 kcal BP that stopped the intermittent desiccation of the wetland. Nevertheless, this amelioration did not result in the full expansion of trees and the low abundance of tree pollen indicates a post-glacial delay in expansion of woodlands. A delayed response is also exhibited in other pollen records from the interior of West Asia such as Lake Van (Wick et al., 2003), Lake Urmia (Bottema, 1986), and Lakes Zeribar and Mirabad (van Zeist and Bottema, 1977) (Fig. 7 F) and further west to Lake Acıgöl in central Turkey (Roberts et al., 2001).

The expansion of grasses together with the low abundance of oak trees can be associated with the amount of moisture during the growing season of these plants. As grasses have a shorter growing period than trees, their sudden expansion against the small presence of trees can indicate a change in the seasonal distribution of precipitation (El-Moslimany, 1986). The presence of adequate moisture during the transition from the cold to the warm season caused the expansion of grasses, but the absence of sufficient moisture in the warm season, i.e., spring and summer, prevented the expansion of oak trees. This interpretation is in agreement with an already proposed change in seasonality of rainfall during the Holocene in the Zagros Mountains based on isotope records of Lakes Zeribar and Mirabad (Stevens et al., 2001). This change in rainfall seasonality has been inferred from depleted isotopic values of the Early Holocene versus enriched values of the Mid-Late Holocene, which is attributed to a higher contribution of isotopically enriched spring rainfall in the second half of the Holocene (Stevens et al., 2001).

Another feature of LPAZ B1 is the appearance and increase in abundance of the ruderal and anthropogenic pollen grains, such as *Centaurea solstitialis*-type and *Carthamus*-type, which could point to degradation of the wetland environment as a result of increased human impact.

LPAZ B2 (6 to 2.2 kcal BP)

The prominent feature of this zone is the increase in the abundance of *Quercus* pollen, which reaches up to 20% at 3.8 kcal BP. The abundance of *Quercus* decreases to 13% from 3.8 to 3 kcal BP and thereafter increases again to 20% at the top of the record. *Pistacia* pollen with an average abundance of 3% is continuously present in this zone. Considering the poor pollen dispersal of *Pistacia* (Wright Jr et al., 1967; van Zeist and Bottema, 1977; Woldring and Bottema, 2003), the trees probably formed a major constituent of the vegetation during this period. Emergence and constant presence of Rosaceae pollen can be associated with a significant presence of wild almond shrubs in habitats where moisture availability did not support the growth of oak trees. The increased abundance of arboreal and shrub pollen along with the decrease in grass pollen abundance, signifies a major change in vegetation from the former grass-dominated steppe-forest to open oak woodlands. Following this change, the abundance of Amaranthaceae pollen declined to its lowest level at the top of the sequence. The appearance of *Fraxinus* pollen during the vegetation shift from steppe-forest to open oak woodlands around 6 kcal BP is a common feature observed in Hashilan and Zeribar pollen records and demonstrates that *Fraxinus* trees occurred on a regional scale. According to Bobek (1951), *Fraxinus* is a riparian element growing along rivers and streams. Hence, its expansion may point to an increase in precipitation in the region leading to increased surface water runoff and fluvial activity, which is in agreement with major vegetation changes recorded in this zone. Another evidence of the increase in humidity is the emergence and continuous presence of *Alisma* pollen at 6 kcal BP. Cyperaceae and *Typha/Sparganium*-type pollen also reached maximum abundance in this zone. Besides the natural vegetation changes, the presence of pollen of *Vitis*, *Centaurea solstitialis*-type, *Carthamus*-type, *Cerealia*-type and probably *Ulmus* indicates intensified human activities.

Discussion

Deglacial climate change in the Zagros Mountains and its link to temperature variability across the North Atlantic

The dominance of an *Artemisia*-Amaranthaceae dry steppe during the period 22-9.8 kcal BP reflects a cold and dry climate in the nearly treeless environment of the Zagros Mountains, which is consistent with the evidence of pollen records from the interior of West Asia such as Lake Urmia (Bottema, 1986; Djamali et al., 2008), Lake Zeribar (van Zeist and Wright, 1963; van Zeist and Bottema, 1977) and Lake Van (Wick et al., 2003; Litt et al., 2009). Insignificant contribution of trees during deglaciation indicates unfavorable conditions for tree growth and most likely an

extremely arid climate (van Zeist and Bottema, 1977). This arid climate is characterized by episodes of enhanced erosion deduced from coarsening of grain size in the calcareous sediments during LGM, HS1 and YD, suggesting amplified aridity during Northern Hemisphere/North Atlantic cooling events. This interpretation is in agreement with the $\delta^{18}O$ record of a stalagmite from SW Zagros Mountains showing increased climate aridity during HS1 and the YD (Soleimani et al., 2022), as well as with intensified dust plumes in West Asia during HS1 and the YD (Pourmand et al., 2004; Sharifi et al., 2018; Safaierad et al., 2020) (Fig. 6). Pollen and sedimentological evidence show a rather humid climate during the B/A interstadial and are consistent with results of diatom analysis (Wasylikowa et al., 2006) and sedimentology (Megard, 1967) of Lake Zeribar, decreased dust input in West Asian terrestrial (Sharifi et al., 2018; Safaierad et al., 2020) and marine records (Pourmand et al., 2004). Thus, our paleoenvironmental record provides further support for a North Atlantic forcing of the West Asian climate.

Out-of-phase moisture variation between the interior of West Asia and the Indian summer monsoon domain during the Holocene

Persistence of steppe vegetation and the emergence of *Ephedra* desert shrubs, lack of expansion of trees, and seasonal desiccation of the Hashilan Wetland indicate the dominance of a warm and dry climate characterized by protracted dry seasons during the Early Holocene in the Zagros Mountains. The similarity of our record with other pollen records from the interior of West Asia (van Zeist and Bottema, 1977; Bottema, 1986; Wick et al., 2003) demonstrates the prevalence of similar bioclimatic conditions throughout this region in the Early Holocene. The dry climate inferred from pollen records is in agreement with the significant activity of dust storms inferred from our MS record. Dust storms maximized between 10.6 and 7.8 kcal BP except for a centennial-scale episode of declined dust input from 9.7 to 9 kcal BP (centered at 9.2 kcal BP). However, such elevated dust deposition in the central Zagros Mountains have not been observed in other dust records from West Asia e.g., Konar Sandal in SE Iran (Safaierad et al., 2020) and Lake Neor in NW Iran (Sharifi et al., 2018), which would point to the occurrence of dust storms on a relatively small spatial scale limited mainly to western Iran.

Comparison of multiproxy evidence from the Hashilan Wetland sediment core with regional records reveals an out-of-phase Holocene moisture variation between the interior of West Asia and the ISM domain. Synchronous with the peak of dust input into the Hashilan Wetland during the Early Holocene (10.6 to 7.8 kcal BP), ISM circulation strengthened and shifted northwards at around 10.5 kcal BP (Fontes et al., 1996; Fleitmann et al., 2003; Gupta et al., 2003; Gupta et al., 2005; Fleitmann et al., 2007; Fuchs and Buerkert, 2008). The ISM remained strong between 10.5

and 7.8 kcal BP and thereafter gradually weakened and migrated southwards. However, the strength of ISM during the Early Holocene was episodically weakened by centennial-scale cold events at 9.2 and 8.2 kcal BP (Neff et al., 2001; Fleitmann et al., 2003; Gupta et al., 2003; Gupta et al., 2005; Dykoski et al., 2005; Fleitmann et al., 2007; Fleitmann et al., 2008; An et al., 2012; Jia et al., 2015). This comparison demonstrates that the increased intensity of the ISM was accompanied by increased climate aridity and elevated dust deposition in the Zagros Mountains.

The driving mechanism of this out-of-phase climate variation is associated with the insolation-driven latitudinal shifts of the Hadley circulation including ISM and STHPs during the Holocene. The Early Holocene boreal summer insolation-maxima on the one hand shifted the summer ITCZ and associated reinforced monsoon circulation northwards (Fleitmann et al., 2003; Fleitmann et al., 2007) and, on the other hand, strengthened and extended the duration of the STHPs over the Zagros Mountains. Moreover, based on the theory of the "monsoon-desert mechanism", the stronger ascending air from the tropical/monsoonal regions is accompanied by stronger descending air in the subtropics ensuing climate aridification (Rodwell and Hoskins, 1996). Under the current climate regime of interior West Asia, the seasonal dominance of the STHPs determines the length of the dry season (Zarrin et al., 2010). Hence, any reconfiguration of atmospheric circulation systems leading to longer dominance of STHPs across the interior of West Asia can prominently change the seasonality of precipitation. Consistently, the Early Holocene reinforcement and northward migration of ISM circulation extended the dominance of the intensified STHPs over the interior of West Asia and thus shifted MLW storm tracks northwards (Sharifi et al., 2018) (Fig. 7, D) with enhanced regional dust emissions. Our evidence and interpretations are in agreement with the results of Djamali et al. (2010) using modern atmospheric data. They demonstrated that the expansion of ISM circulation leads to the establishment of a high-pressure ridge over western/northwestern Iran and eastern Anatolia in late spring. Accordingly, we deduce that the Early Holocene dust storms of our study area occurred in late spring and summer when STHPs dominated the region. This is in agreement with present-day STHPs-driven late spring dust storms in the central Zagros Mountains (Zolfaghari and Abedzadeh, 2005) and also with the similar dust mineral compositions in our record and spring-time dust loads transported from Iraq and the Arabian Peninsula to western Iran (Najafi et al., 2014).

Although the strength of the ISM significantly decreased during both the 9.2 and 8.2 ka cold events, the Hashilan Wetland exhibits quite different dust input during both events. Dust input significantly decreased at 9.2 kcal BP, but reached a maximum at ~8.2 kcal BP and several

centuries earlier. The difference in dust input can be associated with the different configuration of atmospheric systems during these cold spells. The 9.2 ka event, also known as the greatest collapse of the South Asian monsoon system (Zhang et al., 2018), did not significantly influence the high latitudes, whereas the 8.2 ka event has been well recorded in Greenland ice cores (Svensson et al., 2008), implying different cooling mechanisms. We hypothesize that during the 9.2 ka event, due to the weakening and shrinking of ISM circulation, the seasonal dominance of STHPs and thus environmental aridity over the interior of West Asia reduced, resulting in decreased spring/summer dust storms. On the other hand and despite of the weakening of the ISM during the 8.2 ka event, dry MLWs shifted southwards and generated pervasive winter dust storms in West Asia as recorded in dust records from southeastern and northwestern Iran (Sharifi et al., 2018; Safaierad et al., 2020). The dominance of winter atmospheric systems over West Asia is also reflected by the occurrence of the most depleted $\delta^{18}O$ isotope values at 8.2 kcal BP in the Zeribar sediment core, which is attributed to an increase in contribution (concentration) of winter precipitation (Stevens et al., 2001) (Fig. 7 E). Therefore, the peaking dust input to the Hashilan Wetland at around 8.2 kcal BP and several centuries before is associated with a notable contribution of winter dust storms. Indeed, a study of archaeological site abandonment in the Zagros region and beyond also suggests that the effect of the 8.2 ka event was stronger on human communities than the 9.2 ka event (Flohr et al., 2016), an issue we return to below.

The reduced dust input and the gradual increase of oak trees after 7.8 kcal BP indicate an amelioration of the climate synchronous with a gradual decline in boreal summer insolation with a gradual southward migration of the ISM circulation (Neff et al., 2001; Fleitmann et al., 2007) (Fig. 7 A and B). Accordingly, the intensity and dominance of STHPs decreased over the Zagros Mountains and the influence of MLWs increased leading to a shortening of the dry season. The expansion of Zagros oak woodlands continued gradually until 6.3 kcal BP and then suddenly accelerated as recorded by the pollen records of lakes Zeribar (van Zeist and Bottema, 1977) and Van (Wick et al., 2003) (Fig. 7 F). The timing of oak expansion is neatly matched with an abrupt change in the source of moisture for precipitation in northern Oman from the Indian Ocean to more western moisture sources, e.g., the Mediterranean Sea and the North Atlantic Ocean (Fleitmann et al., 2007) (Fig. 7 C). Following this change, the seasonal dominance of MLWs extended over the interior of West Asia allowing the expansion of open oak woodlands across the Zagros-Anti-Taurus Mountains including our site at 6 kcal BP. Moreover, reduced dust input after 6 kcal BP in the Hashilan Wetland point to increasing humidity at the sites of the dust sources in interior West Asia. Our findings from the Hashilan Wetland provide evidence to support the

hypothesis by Djamali et al. (2010) regarding the role of ISM variability on the delayed post-glacial re-expansion of deciduous oak woodlands in the Zagros-Anti-Taurus Mountains.

Human-environment interactions at the dawn of settlements in the Zagros Mountains

Given its proximity to key archaeological sites of the Zagros uplands, the Hashilan Wetland paleoenvironmental record is of special significance for the investigation of long-term human-environment interactions in a sensitive mountain region. Debate has long persisted about the nature of interrelationships between climate, environment and human societies through the course of the Holocene of West Asia with a focus on the significance of climate change for earliest sedentism as an initial stage in the transition from hunter-gatherer to farmer-herder communities (Weninger et al., 2006; Sharifi et al., 2015; Asouti, 2017). Lacustrine sediment records from Lake Zeribar and other sites across Iran agree in suggesting a shift from 15 kcal BP to a warmer, wetter climate, gradually enabling the spread of grass and woodlands to upland zones. The cold and dry conditions of the YD, c. 12.6-11.7 kcal BP, would have had a major impact on the suitability of the high Zagros region for human settlements, even if recent studies indicate at least a sparse human presence by the end of the YD (Matthews et al., 2013; Darabi, 2015). Two palaeohydrobiological records reveal that lake levels were higher in the Late Glacial than during the Early Holocene in NW Iran and southern Zagros possibly due to lower evaporation (Aubert et al., 2017; Aubert et al., 2019). This suggests abundant water resources and their availability to human communities during the YD and at the cultural transition to the onset of the Neolithic.

After the end of the YD, the potential impact of a series of Rapid Climate Change (RCC) events through the Holocene caused by massive melt-water pulses into the North Atlantic (Mayewski et al., 2004) also needs to be considered. While a putative 10.2 ka RCC event appears to have adversely impacted human communities in the Western Fertile Crescent region of Jordan, Israel and western Syria (Weninger et al., 2009; Borrell et al., 2015; Weninger, 2017), our evidence from the Eastern Fertile Crescent (EFC) is insufficient to address this issue. While we need to exercise extreme caution in attributing causality and the shortage of secure and refined dates is a major problem (Flohr et al., 2016), we note that the 9.2 ka RCC event coincides in broad chronological terms with a significant interruption in and relocation of human settlements across the Zagros Mountains. Over the course of the period 9.5-9.0 kcal BP, Early Neolithic settlements at Sheikh-e Abad, Jani, Ganj Dareh, Abdul Hosein and East Chia Sabz in the high Zagros Mountains and at Bestansur and Shimshara in the Iraqi Zagros foothills were all abandoned (Flohr et al., 2020). At approximately the same time, settlements commenced at early farming sites on the lower

plains, including Ali Kosh and Chogha Sefid on the Deh Luran plain, Chogha Bonut on the Susiana plain, and Tappeh Mahtaj on the Behbahan plain (Darabi et al., 2020), all of which were initially settled around c. 9.4-9.2 kcal BP. One scenario, in need of much further research, is that the 9.2 ka event was severe enough to lead to a collapse of agricultural and social systems in the high Zagros Mountains while encouraging the spread of Neolithic communities into lowland zones where cold and drier conditions had less impact and water resources from snow-melt were available. But this highly tentative interpretation needs support from significant refinements of archaeological dating approaches. New evidence from the Hashilan Wetland, however, does not reveal a significant negative impact of climate, at least in terms of aridity, as the 9.2 ka event is situated in the middle of an episode with a decrease in dust suggesting wet and warm climatic conditions.

A further episode of potential significance for the Neolithic of Iran is the 8.2 ka RCC event which, like the YD and the 9.2 ka event, was marked by abrupt cooling and aridity across much of the world (Alley et al., 1997). Neolithic societies in Iran were highly developed by that time with human communities herding animals and cultivating crops since several centuries as well as developing sophisticated resilience strategies involving resource diversification and modes of storage, which could have protected them from worst impacts of RCC events (Clare and Weninger, 2010; Flohr et al., 2016). The most persuasive evidence for significant human behavioral adaptation to the impacts of the 8.2 ka event comes from the Fars region of south-western Iran, where at sites such as Tal-e Mushki and Hormangan a shift from cultivation to hunting is attested by both faunal and stone tool assemblages at c. 8.2-8.0 kcal BP. This is suggesting a possible collapse of local agricultural regimes and a reversion to pre-Neolithic modes of food procurement based on hunting and gathering (Abe and Khanipour, 2019). In contrast to the 9.2 ka event, the 8.2 ka event coincides with a significant episode of maximal dust input attested for the Hashilan Wetland. Arid and cold conditions became a challenge for regional farming communities. Finally, the dependence of agricultural (e.g., dry-farming) and nomado-pastoral practices to the annual distribution of precipitation and changes in continentality suggests that the shift in climate seasonality centered around 6.3 kcal BP would have also had significant implications in understanding cultural changes in the central Zagros.

Conclusions

Pollen and sedimentological evidence from the Hashilan Wetland sediment core provide records of vegetation and climate dynamics in the central Zagros region during the period from 22 to 2.2 kcal BP. Our pollen record confirms the major features of published pollen records including the

dominance of a dry *Artemisia*-Amaranthaceae steppe during the Late Pleistocene persisting until the Early Holocene and a gradual expansion of oak woodlands from the Early to the Mid-Holocene. Our sedimentological results indicate higher transport of calcareous sandy silts into the wetland due to enhanced erosion during LGM, HS1, YD and the 3.2-ka event, providing supporting evidence for the North Atlantic temperature forcing on the West Asian climate.

Comparison of our results with regional paleoclimate records reveals an out-of-phase relationship for Holocene moisture variations between the interior of West Asia and the ISM domain, which is explained by insolation-driven shifts of the Hadley circulation. The Early Holocene increase in boreal summer insolation reinforced and shifted the ISM circulation northwards on the one hand, and strengthened and extended the dominance of the STHPs over the Zagros Mountains on the other hand. This atmospheric configuration protracted the length of the dry season in the interior of West Asia, which is well reflected by seasonal desiccation of the Hashilan Wetland, delayed expansion of the Zagros oak woodlands and increased spring/summer dust input into the study area during the Early Holocene (ca. 11.6 to 7.8 kcal BP). The gradual expansion of oak woodlands and the reduced dust input during the transition from the Early to the Mid-Holocene (7.8 to 6 kcal BP) indicates that the dry season progressively shortened synchronous with a gradual southward migration of the Hadley circulation including STHPs in response to declined summer insolation. In conclusion, our findings provide evidence for the hypothesis presented by Djamali et al. (2010) about the role of ISM variability on post-glacial woodland expansion in the Zagros-Anti-Taurus Mountains. Finally, the Hashilan Wetland record adds further detail to an ever-developing picture of the complex web of human-environment interactions through the course of one of the major transitions in the human narrative, i.e., from mobile hunter-gatherer to sedentary farmer-herder communities.

Acknowledgments

Research underpinning this article was partly funded by an International Partnership and Mobility grant (PM140089) awarded by the British Academy to the University of Reading and the University of Tehran from 2015 to 2018. We are grateful to Arash Sharifi for insightful discussions and comments on an earlier draft of this paper. We thank Dariush Noorollahi and Mohammad Mahdi Abadijoo for their assistance in fieldwork and subsampling the sediment core and Rafael Stiens for analytical support at the GEOPOLAR lab (University of Bremen). The authors are grateful to the editor Neil Roberts and two anonymous reviewers for constructive comments and suggestions that have improved the manuscript.

Data availability statement:

The data that support this study have been published in the PANGAEA data archiving and publication system (Safaierad et al., 2023).

Please add the following reference to your list below. I also added this reference to the start of the methods chapter…

Safaierad, Reza; Zolitschka, Bernd; Djamali, Morteza; Dupont, Lydie M; Vogt, Christoph; Matthews, Roger (2023): Pollen, grain size, loss-on-ignition, elemental and mineralogical composition, magnetic susceptibility and radiocarbon measurements in Hashilan Wetland sediment core. PANGAEA, https://doi.pangaea.de/10.1594/PANGAEA.956292

References

Abe, M., Khanipour, M., 2019. The 8.2 ka Event and Re-microlithization during the Late Mlefaatian in the Zagros Mountains: Analysis of the Flaked Stone Artefacts Excavated from Hormangan in North-eastern Fars, South-west Iran, in: Nakamura, S., Adachi, T., Abe, M. (Eds.), Decades in Deserts: Essays on Near Eastern Archaeology in Honour of Sumio Fujii. Rokuichi Syobou, Tokyo, pp. 305-317.

Aitchison, J., 1982. The statistical analysis of compositional data. Journal of the Royal Statistical Society: Series B (Methodological) 44, 139-160.

Alijani, B., Harman, J.R., 1985. Synoptic climatology of precipitation in Iran. Annals of the Association of American Geographers 75, 404-416.

Alinezhad, K., Ramezani, E., Djamali, M., Sharifi, A., Naqinezhad, A., Aubert, C., Gandouin, E., Pourmand, A., 2021. Lake Neor reveals how mountain vegetation responded to 7000 years of hydroclimate variability in northwestern Iran. Journal of Quaternary Science 36, 598-610.

Alley, R.B., Mayewski, P.A., Sowers, T., Stuiver, M., Taylor, K.C., Clark, P.U., 1997. Holocene climatic instability: A prominent, widespread event 8200 yr ago. Geology 25, 483-486.

Alonso-Zarza, A.M., 2003. Palaeoenvironmental significance of palustrine carbonates and calcretes in the geological record. Earth-Science Reviews 60, 261-298.

Alpert, P., Neumann, J., 1989. An Ancient" Correlation" between Streamflow and Distant Rainfall in the near East. Journal of Near Eastern Studies 48, 313-314.

An, Z., Colman, S.M., Zhou, W., Li, X., Brown, E.T., Jull, A.T., Cai, Y., Huang, Y., Lu, X., Chang, H., 2012. Interplay between the Westerlies and Asian monsoon recorded in Lake Qinghai sediments since 32 ka. Scientific reports 2, 619.

Arsalani, M., Grießinger, J., Bräuning, A., 2022. Tree-ring-based seasonal temperature reconstructions and ecological implications of recent warming on oak forest health in the Zagros Mountains, Iran. International Journal of Biometeorology, 1-13.

Asouti, E., 2017. Human palaeoecology in Southwest Asia during the Early Pre-Pottery Neolithic (c. 9700-8500 cal BC): the plant story, in: Benz, M., Gebel, H.G.K., Watkins, T. (Eds.), Neolithic Corporate Identities. Ex Oriente, Berlin, pp. 21-43.

Aubert, C., Brisset, E., Djamali, M., Sharifi, A., Ponel, P., Gambin, B., Azirani, T.A., Guibal, F., Lahijani, H., Beni, A.N., 2017. Late glacial and early Holocene hydroclimate variability in northwest Iran (Talesh Mountains) inferred from chironomid and pollen analysis. Journal of paleolimnology 58, 151-167.

Aubert, C., Djamali, M., Jones, M., Lahijani, H., Marriner, N., Naderi-Beni, A., Sharifi, A., Ponel, P., Gandouin, E., 2019. A major hydrobiological change in Dasht-e Arjan Wetland (southwestern Iran) during the late glacial–early Holocene transition revealed by subfossil chironomids. Canadian Journal of Earth Sciences 56, 848-856.

Bagheri-Seyedshokri, S., Yamani, M., JafarBigloo, M., karimi, H., Moghimi, E., 2013. Evaluation of hydrodynamic properties of karstic aquifers using time series analysis (Case studies: Karst aquifers of Gilan Gharb and Khorrin in Kermanshah province. Quantitative Geomorphological Research 3, 1-16.

Berger, A., Loutre, M.-F., 1991. Insolation values for the climate of the last 10 million years. Quaternary Science Reviews 10, 297-317.

Blaauw, M., Christen, J.A., 2011. Flexible paleoclimate age-depth models using an autoregressive gamma process. Bayesian analysis 6, 457-474.

Blott, S.J., Pye, K., 2001. GRADISTAT: a grain size distribution and statistics package for the analysis of unconsolidated sediments. Earth surface processes and Landforms 26, 1237-1248.

Bobek, H., 1951. Die naturlichen Walder und Geholzfluren Irans. Bonner Geogr. Abhand. 8, 62S.

Bond, G., Heinrich, H., Broecker, W., Labeyrie, L., McManus, J., Andrews, J., Huon, S., Jantschik, R., Clasen, S., Simet, C., 1992. Evidence for massive discharges of icebergs into the North Atlantic ocean during the last glacial period. Nature 360, 245-249.

Borrell, F., Junno, A., Barceló, J.A., 2015. Synchronous environmental and cultural change in the emergence of agricultural economies 10,000 years ago in the Levant. PloS one 10, e0134810.

Bottema, S., 1986. A late Quaternary pollen diagram from Lake Urmia (northwestern Iran). Review of palaeobotany and palynology 47, 241-261.

Chen, F., Yu, Z., Yang, M., Ito, E., Wang, S., Madsen, D.B., Huang, X., Zhao, Y., Sato, T., Birks, H.J.B., 2008. Holocene moisture evolution in arid central Asia and its out-of-phase relationship with Asian monsoon history. Quaternary Science Reviews 27, 351-364.

Chung, F.H., 1974. Quantitative interpretation of X-ray diffraction patterns of mixtures. I. Matrix-flushing method for quantitative multicomponent analysis. Journal of Applied Crystallography 7, 519-525.

Clare, L., Weninger, B., 2010. Social and biophysical vulnerability of prehistoric societies to Rapid Climate Change. Documenta Praehistorica 37, 283-292.

Croudace, I.W., Löwemark, L., Tjallingii, R., Zolitschka, B., 2019. Current perspectives on the capabilities of high resolution XRF core scanners. Quaternary international 514, 5-15.

Croudace, I.W., Rindby, A., Rothwell, R.G., 2006. ITRAX: description and evaluation of a new multi-function X-ray core scanner. Geological Society, London, Special Publications 267, 51-63.

Darabi, H., 2015. An introduction to the Neolithic revolution of the central Zagros, Iran. Archaeopress.

Darabi, H., Bangsgaard, P., Arranz-Otaegui, A., Ahadi, G., Olsen, J., 2020. Early Neolithic occupation of the lowlands of south-western Iran: new evidence from Tapeh Mahtaj. Antiquity, 1-18.

Dehghani, M., Djamali, M., Gandouin, E., Akhani, H., 2017. A pollen rain-vegetation study along a 3600 m mountain-desert transect in the Irano-Turanian region; implications for the reliability of some pollen ratios as moisture indicators. Review of palaeobotany and palynology 247, 133-148.

Djamali, M., Akhani, H., Andrieu-Ponel, V., Braconnot, P., Brewer, S., de Beaulieu, J.-L., Fleitmann, D., Fleury, J., Gasse, F., Guibal, F., 2010. Indian Summer Monsoon variations could have affected the early-Holocene woodland expansion in the Near East. The Holocene 20, 813-820.

Djamali, M., Akhani, H., Khoshravesh, R., Andrieu-Ponel, V., Ponel, P., Brewer, S., 2011. Application of the global bioclimatic classification to Iran: implications for understanding the modern vegetation and biogeography. Ecologia mediterranea 37, 91-114.

Djamali, M., Baumel, A., Brewer, S., Jackson, S.T., Kadereit, J.W., López-Vinyallonga, S., Mehregan, I., Shabanian, E., Simakova, A., 2012a. Ecological implications of Cousinia Cass.(Asteraceae) persistence through the last two glacial–interglacial cycles in the continental Middle East for the Irano-Turanian flora. Review of Palaeobotany and Palynology 172, 10-20.

Djamali, M., Brewer, S., Breckle, S.W., Jackson, S.T., 2012b. Climatic determinism in phytogeographic regionalization: a test from the Irano-Turanian region, SW and Central Asia. Flora-Morphology, Distribution, Functional Ecology of Plants 207, 237-249.

Djamali, M., de Beaulieu, J.-L., Shah-hosseini, M., Andrieu-Ponel, V., Ponel, P., Amini, A., Akhani, H., Leroy, S.A., Stevens, L., Lahijani, H., 2008. A late Pleistocene long pollen record from Lake Urmia, NW Iran. Quaternary Research 69, 413-420.

Djamali, M., Gondet, S., Ashjari, J., Aubert, C., Brisset, E., Longerey, J., Marriner, N., Mashkour, M., Miller, N.F., Naderi-Beni, A., 2018. Karstic spring wetlands of the Persepolis Basin, southwest Iran: unique sediment archives of Holocene environmental change and human impacts. Canadian journal of earth sciences 55, 1158-1172.

Djamali, M., Jones, M.D., Migliore, J., Balatti, S., Fader, M., Contreras, D., Gondet, S., Hosseini, Z., Lahijani, H., Naderi, A., 2016. Olive cultivation in the heart of the Persian Achaemenid Empire: new insights into agricultural practices and environmental changes reflected in a late Holocene pollen record from Lake Parishan, SW Iran. Vegetation history and archaeobotany 25, 255-269.

Dykoski, C.A., Edwards, R.L., Cheng, H., Yuan, D., Cai, Y., Zhang, M., Lin, Y., Qing, J., An, Z., Revenaugh, J., 2005. A high-resolution, absolute-dated Holocene and deglacial Asian monsoon record from Dongge Cave, China. Earth and Planetary Science Letters 233, 71-86.

El-Moslimany, A.P., 1986. Ecology and late-Quaternary history of the Kurdo-Zagrosian oak forest near Lake Zeribar, western Iran. Vegetatio 68, 55-63.

Erdtman, G., 1960. The acetolysis method-a revised description. Sven Bot Tidskr 54, 516-564.

Faegri, K., Iversen, J., 1989. Textbook of pollen analysis, 4th edn, by Faegri K, Kaland PE, Krzywinski K. Wiley, New York.

Fleitmann, D., Burns, S.J., Mangini, A., Mudelsee, M., Kramers, J., Villa, I., Neff, U., Al-Subbary, A.A., Buettner, A., Hippler, D., 2007. Holocene ITCZ and Indian monsoon dynamics recorded in stalagmites from Oman and Yemen (Socotra). Quaternary Science Reviews 26, 170-188.

Fleitmann, D., Burns, S.J., Mudelsee, M., Neff, U., Kramers, J., Mangini, A., Matter, A., 2003. Holocene forcing of the Indian monsoon recorded in a stalagmite from southern Oman. science 300, 1737-1739.

Fleitmann, D., Mudelsee, M., Burns, S.J., Bradley, R.S., Kramers, J., Matter, A., 2008. Evidence for a widespread climatic anomaly at around 9.2 ka before present. Paleoceanography 23, PA1102.

Flohr, P., Fleitmann, D., Matthews, R., Matthews, W., Black, S., 2016. Evidence of resilience to past climate change in Southwest Asia: Early farming communities and the 9.2 and 8.2 ka events. Quaternary Science Reviews 136, 23-39.

Flohr, P., Matthews, R., Matthews, W., Richardson, A., Fleitmann, D., 2020. Radiocarbon dating of Bestansur and Shimshara, in: Matthews, R., Matthews, W., Richardson, A. (Eds.), The

Early Neolithic of the Eastern Fertile Crescent: Excavations at Bestansur and Shimshara, Iraqi Kurdistan CZAP Reports 2. Oxford: Oxbow, pp. 187-195.

Folk, R.L., Ward, W.C., 1957. Brazos River bar [Texas]; a study in the significance of grain size parameters. Journal of sedimentary research 27, 3-26.

Fontes, J.-C., Gasse, F., Gibert, E., 1996. Holocene environmental changes in Lake Bangong basin (Western Tibet). Part 1: Chronology and stable isotopes of carbonates of a Holocene lacustrine core. Palaeogeography, Palaeoclimatology, Palaeoecology 120, 25-47.

Fuchs, M., Buerkert, A., 2008. A 20 ka sediment record from the Hajar Mountain range in N-Oman, and its implication for detecting arid–humid periods on the southeastern Arabian Peninsula. Earth and Planetary Science Letters 265, 546-558.

Glenn, E., Thompson, T.L., Frye, R., Riley, J., Baumgartner, D., 1995. Effects of salinity on growth and evapotranspiration of Typha domingensis Pers. Aquatic Botany 52, 75-91.

Griffiths, H.I., Schwalb, A., Stevens, L.R., 2001. Evironmental change in southwestern Iran: the Holocene ostracod fauna of Lake Mirabad. The Holocene 11, 757-764.

Grimm, E., 2011. TILIA 1.7. 16. Illinois State Museum. Research and Collection Center.

Grimm, E.C., 1987. CONISS: a FORTRAN 77 program for stratigraphically constrained cluster analysis by the method of incremental sum of squares. Computers & geosciences 13, 13-35.

Gupta, A.K., Anderson, D.M., Overpeck, J.T., 2003. Abrupt changes in the Asian southwest monsoon during the Holocene and their links to the North Atlantic Ocean. Nature 421, 354.

Gupta, A.K., Das, M., Anderson, D.M., 2005. Solar influence on the Indian summer monsoon during the Holocene. Geophysical Research Letters 32, L17703.

Gurjazkaite, K., Routh, J., Djamali, M., Vaezi, A., Poher, Y., Beni, A.N., Tavakoli, V., Kylin, H., 2018. Vegetation history and human-environment interactions through the late Holocene in Konar Sandal, SE Iran. Quaternary Science Reviews 194, 143-155.

Hamzeh, M.A., Gharaie, M.H.M., Lahijani, H.A.K., Djamali, M., Harami, R.M., Beni, A.N., 2016. Holocene hydrological changes in SE Iran, a key region between Indian summer monsoon and Mediterranean winter precipitation zones, as revealed from a lacustrine sequence from Lake Hamoun. Quaternary International 408, 25-39.

Heinrich, H., 1988. Origin and consequences of cyclic ice rafting in the northeast Atlantic Ocean during the past 130,000 years. Quaternary research 29, 142-152.

Heiri, O., Lotter, A.F., Lemcke, G., 2001. Loss on ignition as a method for estimating organic and carbonate content in sediments: reproducibility and comparability of results. Journal of paleolimnology 25, 101-110.

Howard, A.J., Gearey, B.R., Hill, T., Fletcher, W., Marshall, P., 2009. Fluvial sediments, correlations and palaeoenvironmental reconstruction: the development of robust radiocarbon chronologies. Journal of Archaeological Science 36, 2680-2688.

Jafarbigloo, M., Veysi, A., Nuraeesefat, I., Naderi, S., 2015. Study of drought impact assessment on Hashiland Wetland. Wetland Ecobiology 7, 81-92.

Jia, G., Bai, Y., Yang, X., Xie, L., Wei, G., Ouyang, T., Chu, G., Liu, Z., Peng, P.a., 2015. Biogeochemical evidence of Holocene East Asian summer and winter monsoon variability from a tropical maar lake in southern China. Quaternary Science Reviews 111, 51-61.

Jones, M.D., Abu‐Jaber, N., AlShdaifat, A., Baird, D., Cook, B.I., Cuthbert, M.O., Dean, J.R., Djamali, M., Eastwood, W., Fleitmann, D., 2019. 20,000 years of societal vulnerability and adaptation to climate change in southwest Asia. Wiley Interdisciplinary Reviews: Water 6, e1330.

Kaniewski, D., Marriner, N., Cheddadi, R., Morhange, C., Bretschneider, J., Jans, G., Otto, T., Luce, F., Van Campo, E., 2019. Cold and dry outbreaks in the eastern Mediterranean 3200 years ago. Geology 47, 933-937.

Khoshakhlagh, F., Ouji, R., Jafarbeglou, M., 2008. A synoptic study on seasonal patterns of wet and dry spells in midwest of Iran. Desert 13, 89-103.

Khoshakhlagh, F., Safaierad, R., Salmani, D., 2014. The Synoptic analysis of flood occurrence on November 2011 in Behbahan and Likak cities. Physical Geography Research Quarterly 46, 509-524.

Köppen, W., 1931. Grundriss der Klimakunde (Outline of climate science). Walter de Gruyter, Berlin, 388pp. map.

Kumar, A., Suresh, K., Rahaman, W., 2020. Geochemical characterization of modern aeolian dust over the Northeastern Arabian Sea: Implication for dust transport in the Arabian Sea. Science of The Total Environment 729, 138576.

Litt, T., Krastel, S., Sturm, M., Kipfer, R., Örcen, S., Heumann, G., Franz, S.O., Ülgen, U.B., Niessen, F., 2009. 'PALEOVAN', International Continental Scientific Drilling Program (ICDP): site survey results and perspectives. Quaternary Science Reviews 28, 1555-1567.

Martin‐Puertas, C., Tjallingii, R., Bloemsma, M., Brauer, A., 2017. Varved sediment responses to early Holocene climate and environmental changes in Lake Meerfelder Maar (Germany) obtained from multivariate analyses of micro X‐ray fluorescence core scanning data. Journal of Quaternary Science 32, 427-436.

Matthews, R., Matthews, W., Raheem, K.R., Richardson, A., 2020. The Early Neolithic of the Eastern Fertile Crescent: Excavations at Bestansur and Shimshara, Iraqi Kurdistan. Oxbow.

Matthews, R., Nashli, H.F., 2013. The Neolithisation of Iran. Oxbow Books.

Matthews, R.J., Matthews, W., Richardson, A., 2013. Radiocarbon dating of Sheikh-e Abad and Jani, in: Matthews, R., Matthews, W., Mohammadifar, Y. (Eds.), The Earliest Neolithic of Iran: 2008 Excavations at Sheikh-e Abad and Jani. CZAP Reports 1. Oxford: Oxbow, pp. 61-65.

Mayewski, P.A., Rohling, E.E., Stager, J.C., Karlén, W., Maasch, K.A., Meeker, L.D., Meyerson, E.A., Gasse, F., van Kreveld, S., Holmgren, K., 2004. Holocene climate variability. Quaternary research 62, 243-255.

Megard, R.O., 1967. Late‐Quaternary Cladocera of Lake Zeribar Western Iran. Ecology 48, 179-189.

Molloy, B., 2022. Was There a 3.2 ka Crisis in Europe? A Critical Comparison of Climatic, Environmental, and Archaeological Evidence for Radical Change during the Bronze Age–Iron Age Transition. Journal of Archaeological Research, 1-64.

Najafi, M.S., Khoshakhllagh, F., Zamanzadeh, S.M., Shirazi, M.H., Samadi, M., Hajikhani, S., 2014. Characteristics of TSP loads during the Middle East springtime dust storm (MESDS) in Western Iran. Arabian Journal of Geosciences 7, 5367-5381.

Neff, U., Burns, S., Mangini, A., Mudelsee, M., Fleitmann, D., Matter, A., 2001. Strong coherence between solar variability and the monsoon in Oman between 9 and 6 kyr ago. Nature 411, 290.

Neumann, J., Parpola, S., 1987. Climatic change and the eleventh-tenth-century eclipse of Assyria and Babylonia. Journal of Near Eastern Studies 46, 161-182.

Pourmand, A., Marcantonio, F., Schulz, H., 2004. Variations in productivity and eolian fluxes in the northeastern Arabian Sea during the past 110 ka. Earth and Planetary Science Letters 221, 39-54.

Profe, J., Ohlendorf, C., 2019. X-ray fluorescence scanning of discrete samples–An economical perspective. Quaternary International 514, 68-75.

R Development Core Team, R., 2013. R: A language and environment for statistical computing.

Reimer, P.J., Austin, W.E., Bard, E., Bayliss, A., Blackwell, P.G., Ramsey, C.B., Butzin, M., Cheng, H., Edwards, R.L., Friedrich, M., 2020. The IntCal20 Northern Hemisphere radiocarbon age calibration curve (0–55 cal kBP). Radiocarbon 62, 725-757.

Roberts, N., Reed, J., Leng, M., Kuzucuoğlu, C., Fontugne, M., Bertaux, J., Woldring, H., Bottema, S., Black, S., Hunt, E., 2001. The tempo of Holocene climatic change in the eastern Mediterranean region: new high-resolution crater-lake sediment data from central Turkey. The Holocene 11, 721-736.

Rodwell, M.J., Hoskins, B.J., 1996. Monsoons and the dynamics of deserts. Quarterly Journal of the Royal Meteorological Society 122, 1385-1404.

Safaierad, R., Azizi, G., Maghsoudi, M., 2018. The role of changes in the large-scale atmospheric systems in the evolution of the late Pleistocene and Holocene climate of the Zagros Mountains. Quaternery Journal of Iran 4, 253-271.

Safaierad, R., Mohtadi, M., Zolitschka, B., Yokoyama, Y., Vogt, C., Schefuß, E., 2020. Elevated dust depositions in West Asia linked to ocean–atmosphere shifts during North Atlantic cold events. Proceedings of the National Academy of Sciences 117, 18272-18277.

Shaikh Baikloo Islam, B., 2021. Southwest Asia during the Iron Age from the perspective of climatic events. Journal of Iran's Pre Islamic Archaeological Essays 5, 63-76.

Sharifi, A., Murphy, L.N., Pourmand, A., Clement, A.C., Canuel, E.A., Beni, A.N., Lahijani, H.A., Delanghe, D., Ahmady-Birgani, H., 2018. Early-Holocene greening of the Afro-Asian dust belt changed sources of mineral dust in West Asia. Earth and Planetary Science Letters 481, 30-40.

Sharifi, A., Pourmand, A., Canuel, E.A., Ferer-Tyler, E., Peterson, L.C., Aichner, B., Feakins, S.J., Daryaee, T., Djamali, M., Beni, A.N., 2015. Abrupt climate variability since the last deglaciation based on a high-resolution, multi-proxy peat record from NW Iran: The hand that rocked the Cradle of Civilization? Quaternary Science Reviews 123, 215-230.

Soleimani, M., Nadimi, A., Koltai, G., Dublyansky, Y., Carolin, S., Spötl, C., 2022. Stalagmite evidence of Last Glacial Maximum to early Holocene climate variability in southwestern Iran. Journal of Quaternary Science.

Stevens, L., Wright Jr, H., Ito, E., 2001. Proposed changes in seasonality of climate during the Lateglacial and Holocene at Lake Zeribar, Iran. The Holocene 11, 747-755.

Stevens, L.R., Ito, E., Schwalb, A., Wright, H.E., 2006. Timing of atmospheric precipitation in the Zagros Mountains inferred from a multi-proxy record from Lake Mirabad, Iran. Quaternary research 66, 494-500.

Svensson, A., Andersen, K.K., Bigler, M., Clausen, H.B., Dahl-Jensen, D., Davies, S., Johnsen, S.J., Muscheler, R., Parrenin, F., Rasmussen, S.O., 2008. A 60 000 year Greenland stratigraphic ice core chronology. Climate of the Past 4, 47-57.

Talebi, T., Ramezani, E., Djamali, M., Lahijani, H.A.K., Naqinezhad, A., Alizadeh, K., Andrieu-Ponel, V., 2016. The Late-Holocene climate change, vegetation dynamics, lake-level changes and anthropogenic impacts in the Lake Urmia region, NW Iran. Quaternary International 408, 40-51.

Tjallingii, R., Röhl, U., Kölling, M., Bickert, T., 2007. Influence of the water content on X‐ray fluorescence core‐scanning measurements in soft marine sediments. Geochemistry, Geophysics, Geosystems 8.

Vaezi, A., Ghazban, F., Tavakoli, V., Routh, J., Beni, A.N., Bianchi, T.S., Curtis, J.H., Kylin, H., 2019. A Late Pleistocene-Holocene multi-proxy record of climate variability in the Jazmurian playa, southeastern Iran. Palaeogeography, palaeoclimatology, palaeoecology 514, 754-767.

Vaezi, A., Routh, J., Djamali, M., Gurjazkaite, K., Tavakoli, V., Beni, A.N., Roberts, P., 2022. New multi-proxy record shows potential impacts of precipitation on the rise and ebb of Bronze Age and imperial Persian societies in southeastern Iran. Quaternary Science Reviews 298, 107855.

van Zeist, W., Bottema, S., 1977. Palynological investigations in western Iran. Palaeohistoria, 19-85.

van Zeist, W., Wright, H.E., 1963. Preliminary pollen studies at Lake Zeribar, Zagros mountains, southwestern Iran. Science 140, 65-67.

Wasylikowa, K., 1967. Late quaternary plant macrofossils from Lake Zeribar, western Iran. Review of Palaeobotany and Palynology 2, 313-318.

Wasylikowa, K., Witkowski, A., Walanus, A., Hutorowicz, A., Alexandrowicz, S.W., Langer, J.J., 2006. Palaeolimnology of Lake Zeribar, Iran, and its climatic implications. Quaternary Research 66, 477-493.

Weltje, G.J., Bloemsma, M., Tjallingii, R., Heslop, D., Röhl, U., Croudace, I.W., 2015. Prediction of geochemical composition from XRF core scanner data: a new multivariate approach including automatic selection of calibration samples and quantification of uncertainties, Micro-XRF studies of sediment cores. Springer, pp. 507-534.

Weninger, B., Alram-Stern, E., Bauer, E., Clare, L., Danzeglocke, U., Jöris, O., Kubatzki, C., Rollefson, G., Todorova, H., van Andel, T., 2006. Climate forcing due to the 8200 cal yr BP event observed at Early Neolithic sites in the eastern Mediterranean. Quaternary Research 66, 401-420.

Weninger, B., Clare, L., Rohling, E., Bar-Yosef, O., Böhner, U., Budja, M., Bundschuh, M., Feurdean, A., Gebe, H.G., Jöris, O., 2009. The impact of rapid climate change on prehistoric societies during the Holocene in the Eastern Mediterranean. Documenta praehistorica 36, 7-59.

Weninger, B.P., 2017. Niche construction and theory of agricultural origins. Case studies in punctuated equilibrium. Documenta Praehistorica 44, 6-17.

White, F., Léonard, J., 1991. Phytogeographical links between Africa and southwest Asia. Flora et Vegetatio Mundi 9, 229-246.

Wick, L., Lemcke, G., Sturm, M., 2003. Evidence of Lateglacial and Holocene climatic change and human impact in eastern Anatolia: high-resolution pollen, charcoal, isotopic and geochemical records from the laminated sediments of Lake Van, Turkey. The Holocene 13, 665-675.

Woldring, H., Bottema, S., 2003. The vegetation history of East-Central Anatolia in relation to archaeology: the Eski Acıgöl pollen evidence compared with the Near Eastern environment. Palaeohistoria 44, 1-34.

Wright Jr, H., McAndrews, J.H., van Zeist, W., 1967. Modern pollen rain in western Iran, and its relation to plant geography and Quaternary vegetational history. The Journal of Ecology, 415-443.

Wright Jr, H.E., 1962. Pleistocene glaciation in Kurdistan. E&G–Quaternary Science Journal 12, 131-164.

Zarrin, A., Ghaemi, H., Azadi, M., Farajzadeh, M., 2010. The spatial pattern of summertime subtropical anticyclones over Asia and Africa: A climatological review. International Journal of Climatology: A Journal of the Royal Meteorological Society 30, 159-173.

Zhang, W., Yan, H., Dodson, J., Cheng, P., Liu, C., Li, J., Lu, F., Zhou, W., An, Z., 2018. The 9.2 ka event in Asian summer monsoon area: the strongest millennial scale collapse of the monsoon during the Holocene. Climate dynamics 50, 2767-2782.

Zohary, M., 1973. Geobotanical foundations of the Middle East. Fischer, Stuttgart.

Zolfaghari, H., Abedzadeh, H., 2005. Synoptic analysis of dust systems in the West of Iran. J Geogr Dev (Iran) 6, 173-188.

1095

1100

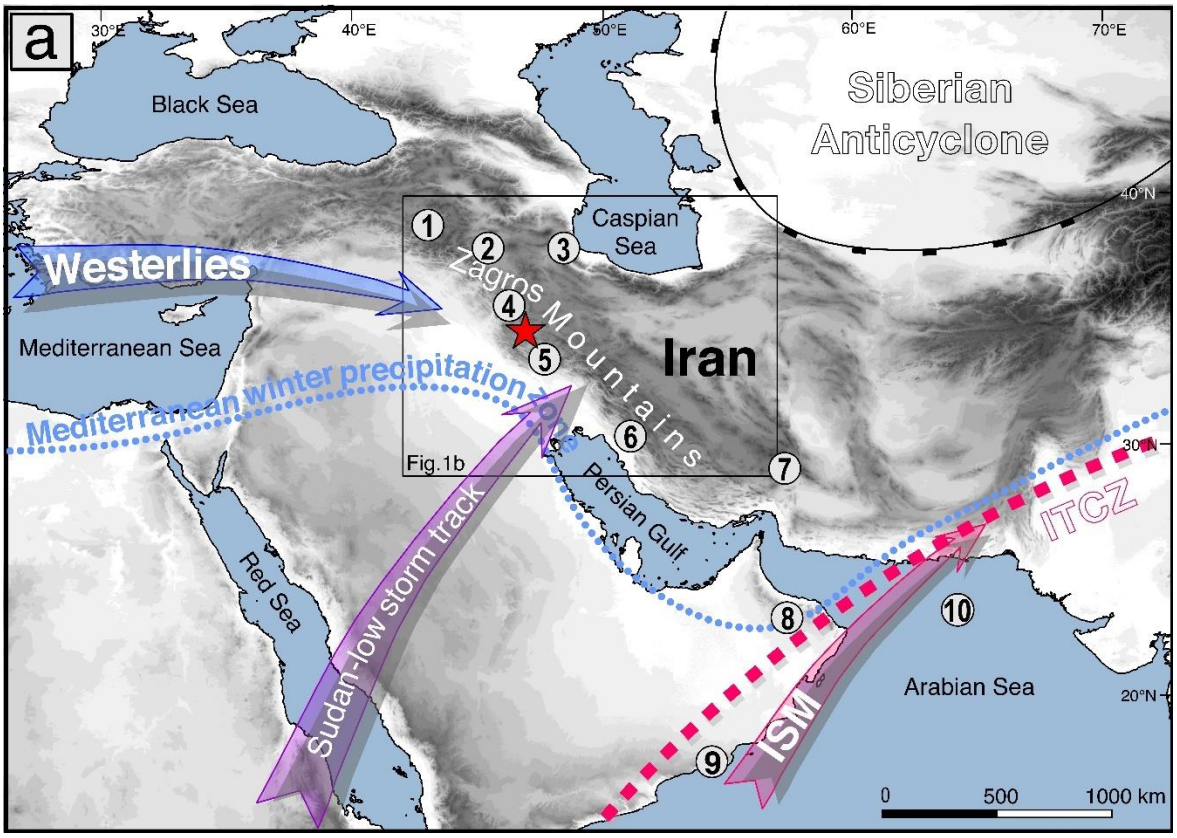
a
30°E
40°E
50°E
60°E
70°E
Black Sea
Siberian
Anticyclone
40°N
Caspian
Sea
1
2
3
Westerlies
Zagros Mountains
4
5
Iran
Mediterranean Sea
Mediterranean winter precipitation
6
Fig.1b
7
Persian Gulf
ITCZ
30°N
Red Sea
Sudan-low storm track
8
10
Arabian Sea
20°N
ISM
9
0
500
1000 km

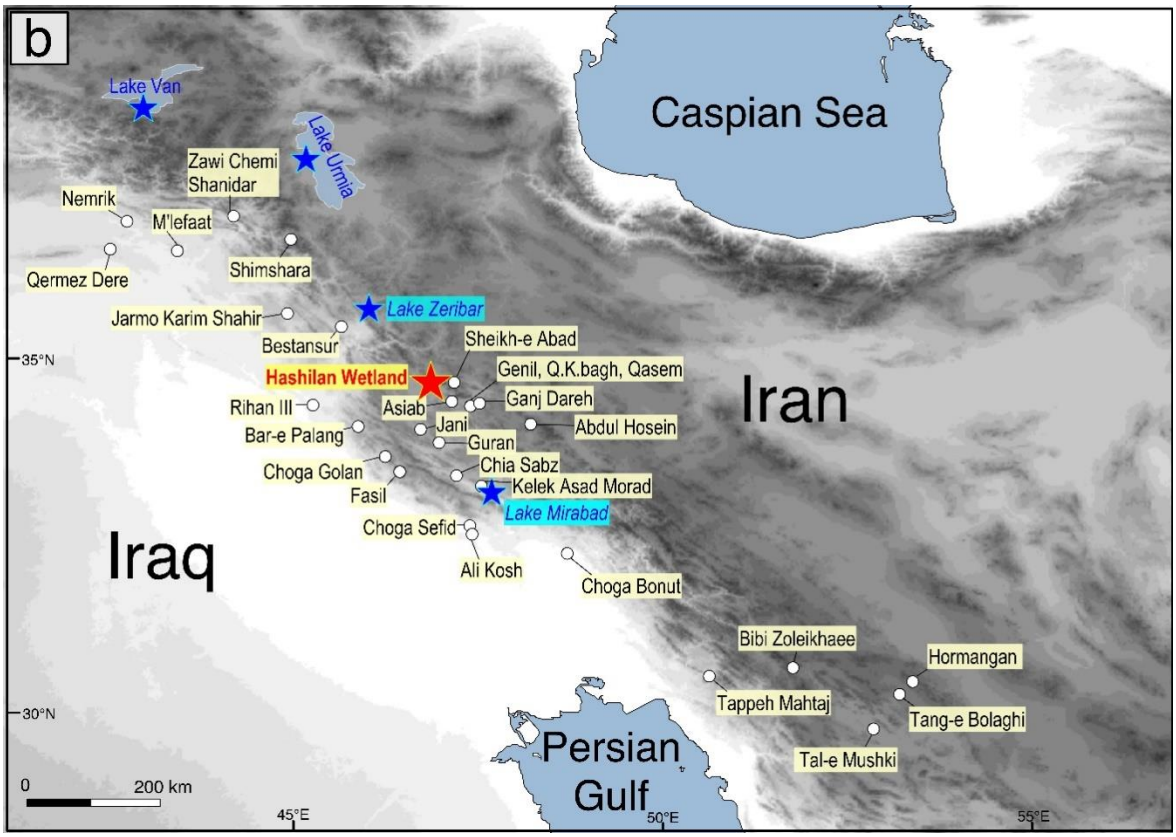

Fig. 1. **a**. Map of West Asia with dominant synoptic systems (after Chen et al. (2008); ISM: Indian Summer Monsoon, ITCZ: Intertropical Convergence Zone). Red star shows the position of Hashilan Wetland (this study). Numbers within the gray circles correspond to locations with paleoenvironmental studies in West Asia mentioned in this paper: 1. Lake Van (Wick et al., 2003), 2. Lake Urmia (Bottema, 1986), 3. Lake Neor (Sharifi et al., 2015), 4. Lake Zeribar (van Zeist and Wright, 1963; van Zeist and Bottema, 1977), 5. Lake Mirabad (van Zeist and Bottema, 1977; Stevens et al., 2006), 6. Sibaki Cave (Soleimani et al., 2022), 7. Konar Sandal peat bog (Safaierad et al., 2020), 8. Hoti Cave (Fleitmann et al., 2007), 9. Qunf Cave (Fleitmann et al., 2003), and 10. Marine sediment core 93KL from the Arabian Sea (Pourmand et al., 2004). **b**. Locations of Early Neolithic sites across the Zagros Mountain range and nearby lowlands (modified after Matthews and Nashli (2013)).

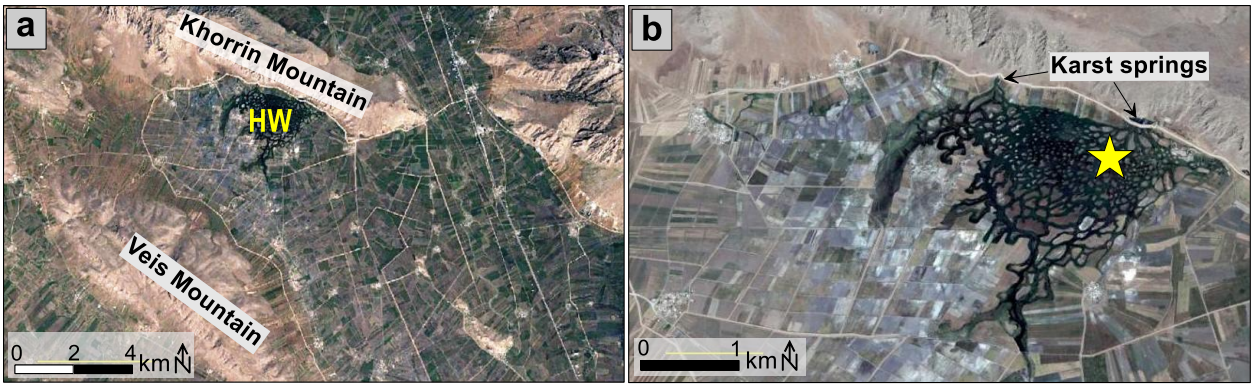

Fig. 2. a. Satellite image of the Hashilan Wetland (HW) and its surrounding limestone catchment (Google Earth: 6 February 2019). **b**. Satellite image of the island-like surface of Hashilan Wetland with location of coring (yellow star) and karst springs (Google Earth: 14 June 2019).

1125

1130

1135

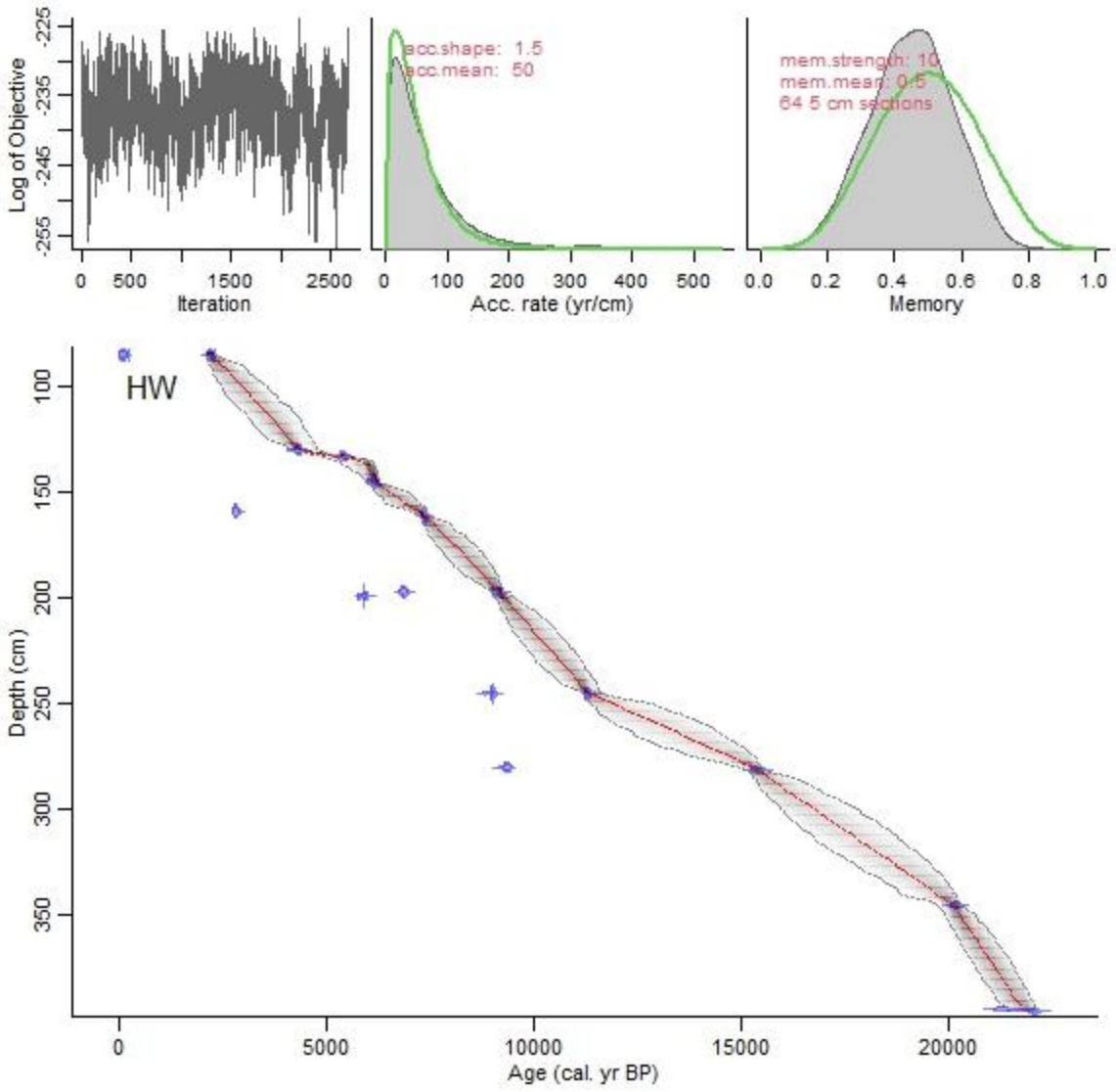

Fig. 3. Bayesian age-depth model for the Hashilan sediment core. In blue: distribution of individual dates. The best model is shown by the red dotted line and the 95% probability interval by the shaded area between grey dotted lines. The upper part shows the Markov chain Monte Carlo (MCMC) iterations (left), the prior (green) and posterior (grey) distributions for the accumulation rate (middle), and memory (right).

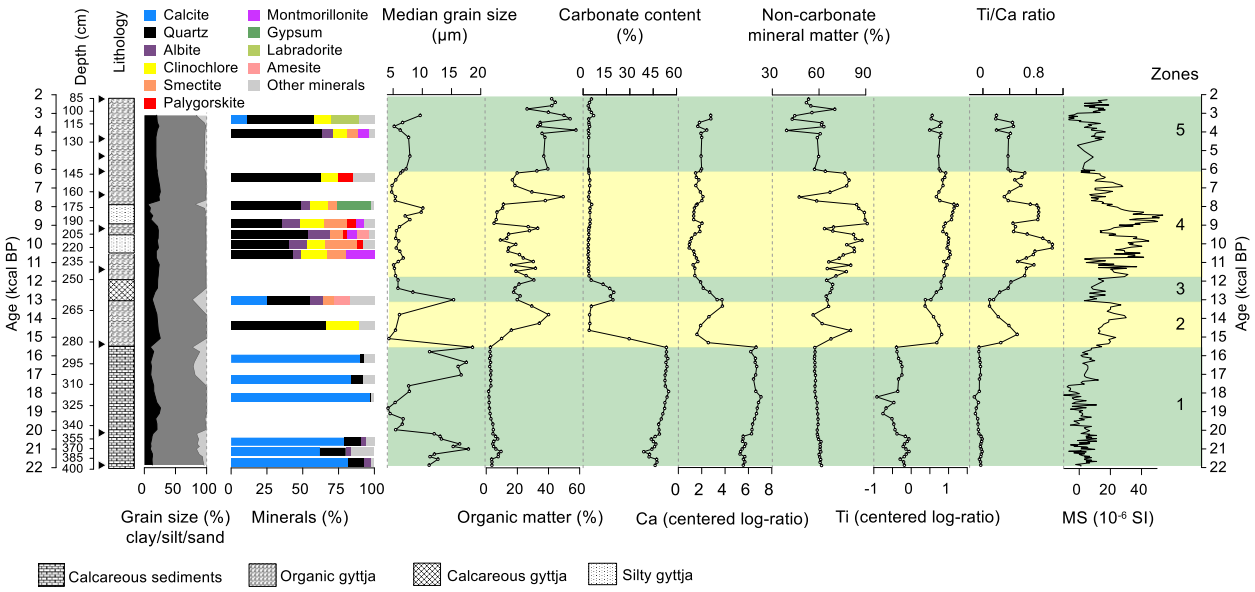

Fig. 4. Lithology and downcore variations in grain size, mineral abundances, median grain size, organic matter, carbonate content, calcium (Ca), non-carbonate mineral matter, titanium (Ti), Ti/Ca ratio, and magnetic susceptibility (MS). Black triangles along the lithology indicate the position of ^{14}C age controls for the sediment core. Sediment zones 1-5 are color-shaded.

1155

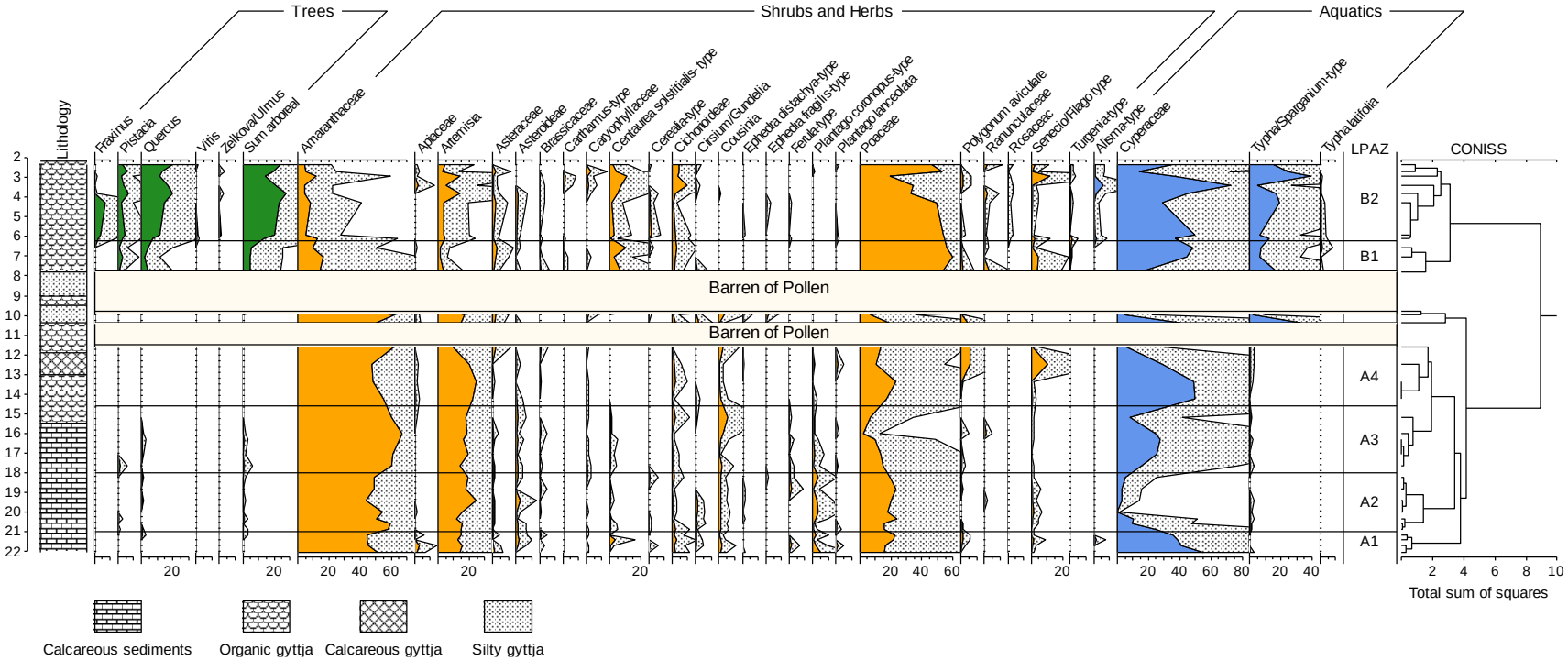

Fig. 5. Pollen percentage diagram of selected taxa from the Hashilan Wetland sediment core along with local pollen assemblage zones (LPAZ) defined by CONISS. The dotted shading denotes 5x exaggeration of the original values (in %).

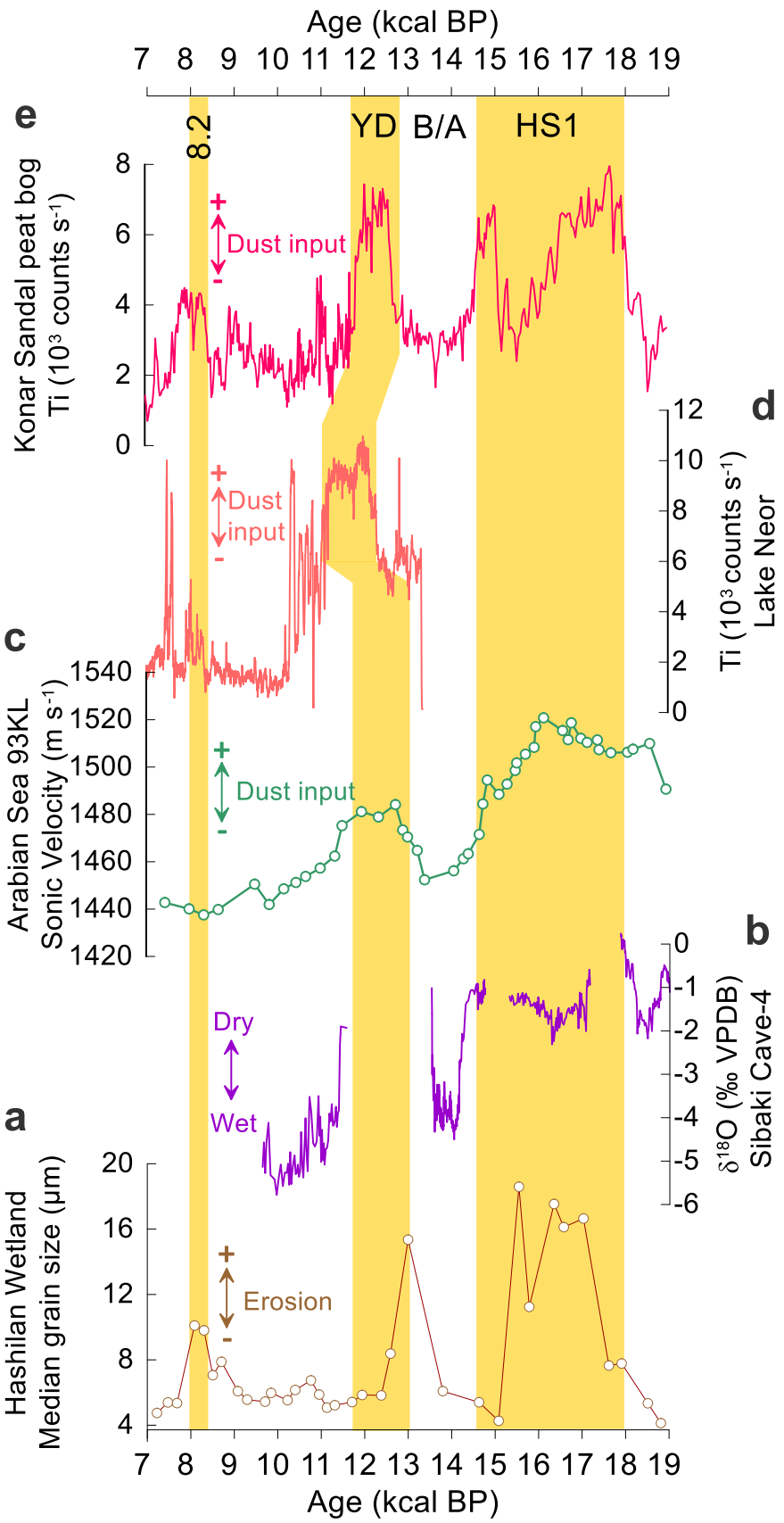
Age (kcal BP)
7 8 9 10 11 12 13 14 15 16 17 18 19
8.2
YD
B/A
HS1
e
Konar Sandal peat bog
Ti (10³ counts s⁻¹)
Dust input
d
Ti (10³ counts s⁻¹)
Lake Neor
Dust input
c
Arabian Sea 93KL
Sonic Velocity (m s⁻¹)
Dust input
b
δ¹⁸O (‰ VPDB)
Sibaki Cave-4
Dry
Wet
a
Hashilan Wetland
Median grain size (μm)
Erosion
Age (kcal BP)

Fig. 6. Comparison of the Hashilan Wetland mean grain size record as a proxy for enhanced erosion (a), with paleoclimate records from West Asia: (b) $\delta^{18}O$ record of Sibaki Cave in the SW Zagros Mountains (Soleimani et al., 2022), (c) Sonic velocity at core 93KL from the Arabian Sea (Pourmand et al., 2004), (d) Ti record of a sediment core from Lake Neor (Sharifi et al., 2018), and (e) Ti record of a sediment core from Konar Sandal peat bog (Safaierad et al., 2020). HS1: Heinrich Stadial 1, B/A: Bølling–Allerød, YD: Younger Dryas, and 8.2: 8.2 ka event.

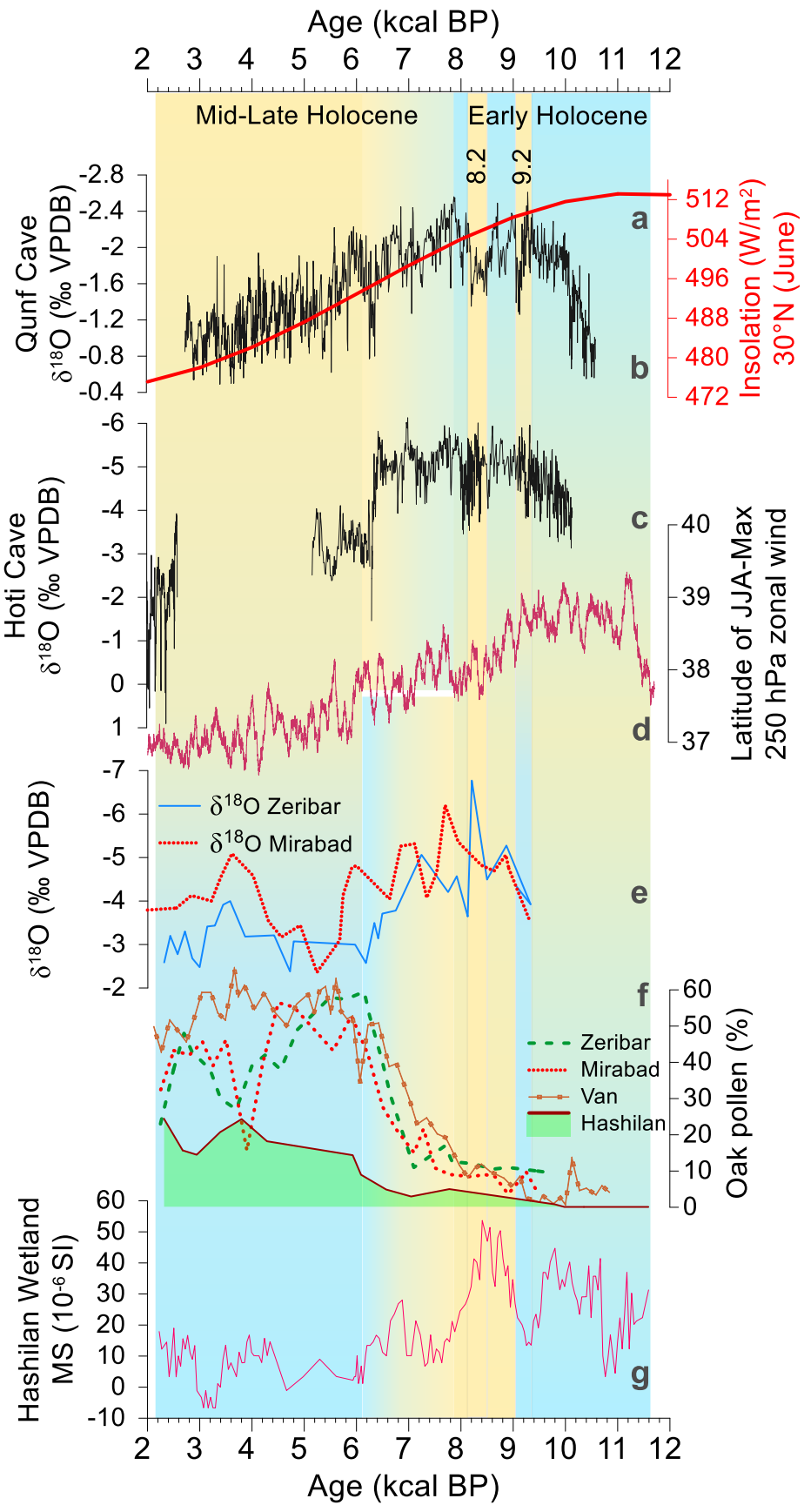
Age (kcal BP)
2 3 4 5 6 7 8 9 10 11 12
Mid-Late Holocene
Early Holocene
8.2
9.2
Qunf Cave
δ18O (‰ VPDB)
-2.8 -2.4 -2 -1.6 -1.2 -0.8 -0.4
a
b
512 504 496 488 480 472
Insolation (W/m2)
30°N (June)
Hoti Cave
δ18O (‰ VPDB)
-6 -5 -4 -3 -2 -1 0 1
c
d
40 39 38 37
Latitude of JJA-Max
250 hPa zonal wind
δ18O (‰ VPDB)
-7 -6 -5 -4 -3 -2
δ18O Zeribar
δ18O Mirabad
e
f
Zeribar
Mirabad
Van
Hashilan
60 50 40 30 20 10 0
Oak pollen (%)
Hashilan Wetland
MS (10-6 SI)
60 50 40 30 20 10 0 -10
g
2 3 4 5 6 7 8 9 10 11 12
Age (kcal BP)

Fig. 7. **a**. Summer insolation curve (June) for 30° N (Berger and Loutre, 1991). **b**. Qunf Cave stalagmite $\delta^{18}O$ from southern Oman (Fleitmann et al., 2003), and **c**. Hoti Cave stalagmite $\delta^{18}O$ from northern Oman (Fleitmann et al., 2007), a proxy for ISM rainfall variations. **d**. A Hovmöller plot of mean June–July–August zonal wind maximum (JJA-Max) at 250hPa (U250_max) averaged longitudinally between 30–60° E in the Trace experiment (Sharifi et al., 2018). **e**. Oxygen isotope profiles of Zeribar and Mirabad lakes (Stevens et al., 2001; Stevens et al., 2006). **f**. Oak pollen records for Zeribar and Mirabad lakes (van Zeist and Bottema, 1977), Lake Van (Wick et al., 2003), and Hashilan Wetland (this study). **g**. Magnetic susceptibility record of Hashilan Wetland (this study). Blue and yellow shadings indicate wet and dry climate intervals, respectively. 9.2: 9.2 ka event, and 8.2: 8.2 ka event.

Table 1. Radiocarbon ages and calibrated dates.

Lab. Code	Depth (cm)	Material dated	^{14}C age (BP)	95% confidence interval (cal. BP)	Midpoint of calibrated age (cal. BP)	Outlier
Beta-468207	85	Phragmites rhizome	90±30	90	95	X
Beta-482658	85	Organic sediment	2230±30	2110 - 2330	2220	
Beta-617921	130	Charcoal	3890±30	4140 - 4795	4350	
Beta-484596	133	Organic sediment	4680±30	4900 - 5420	5285	
Beta-486781	145	Organic sediment	5370±30	6020 - 6290	6100	
Beta-468206	159	Phragmites rhizome	2740 ± 30	2855 - 2790	2820	X
Beta-482659	161	Organic sediment	6480±30	7250 - 7470	7360	
Beta-484248	197	Phragmites rhizome	6030 ± 30	6951 - 6789	6870	X
Beta-482660	197	Organic sediment	8200±30	9025 - 9280	9170	
Beta-468205	199	Phragmites rhizome	5150 ± 30	5940 - 5895	5920	X
Beta-482661	245	Organic sediment	9910±30	11210 - 11670	11360	
Beta-484249	245	Phragmites rhizome	8090 ± 30	9094 - 8985	9040	X
Beta-468203	280	Phragmites rhizome	8340 ± 30	9452 - 9287	9370	X
Beta-482662	281	Organic sediment	12880±40	15150 - 15580	15370	
Beta-484597	345	Organic sediment	16700±40	19720 - 20330	20120	
Beta-617926	394	Cyperaceae seeds	17650±60	21400 - 22115	21825	
Beta-482663	395	Organic sediment	18130±60	21430 - 22150	21860	

Table 2. Correlation matrix of centered log-ratio (clr) transformed elemental data from the Hashilan Sediment core. High correlations (r > 0.8 or <-0.8) are marked with bold numbers.

	Ca-clr	*Ti-clr*	*Cr-clr*	*Mn-clr*	*Fe-clr*	*Ni-clr*	*Zn-clr*	*Rb-clr*	*Sr-clr*	*Zr-clr*
Ca-clr	**1**									
Ti-clr	**-0.93**	**1**								
Cr-clr	-0.57	0.67	**1**							
Mn-clr	**-0.86**	**0.87**	0.48	**1**						
Fe-clr	**-0.85**	**0.92**	0.53	**0.87**	**1**					
Ni-clr	**-0.84**	**0.88**	0.65	0.74	**0.89**	**1**				
Zn-clr	-0.61	0.61	0.48	0.49	0.40	0.49	**1**			
Rb-clr	-0.55	0.22	-0.12	0.30	0.19	0.19	0.15	**1**		
Sr-clr	**0.99**	**-0.89**	-0.51	**-0.87**	**-0.82**	**-0.80**	-0.62	-0.60	**1**	
Zr-clr	**-0.82**	**0.90**	0.65	0.76	**0.80**	0.75	0.59	0.17	**-0.82**	**1**